AD-A136 377 SIMULATION OF THEMATIC MAPPER DATA FOR REMOTE BATHYMETRY(U) ENVIRONMENTAL RESEARCH INST OF MICHIGAN ANN ARBOR APPLICATIONS DIV F J TANIS ET AL. OCT 83 1/1

UNCLASSIFIED ERIM-163100-7-F N00014-82-C-2311 F/G 8/10 NL

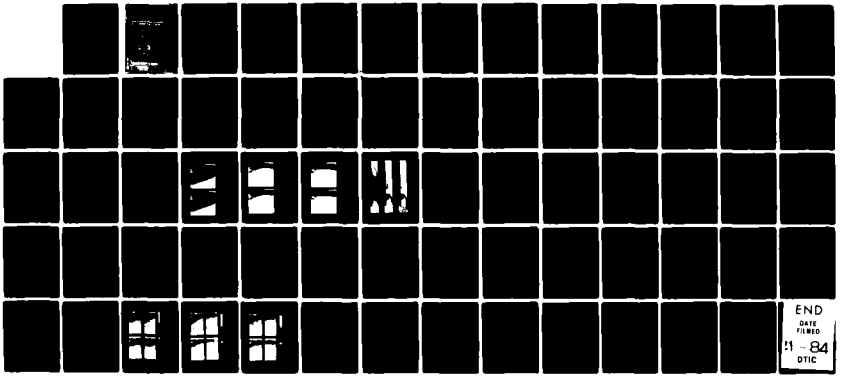

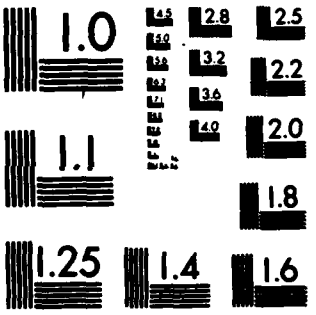

MICROCOPY RESOLUTION TEST CHART
NATIONAL BUREAU OF STANDARDS-1963-A

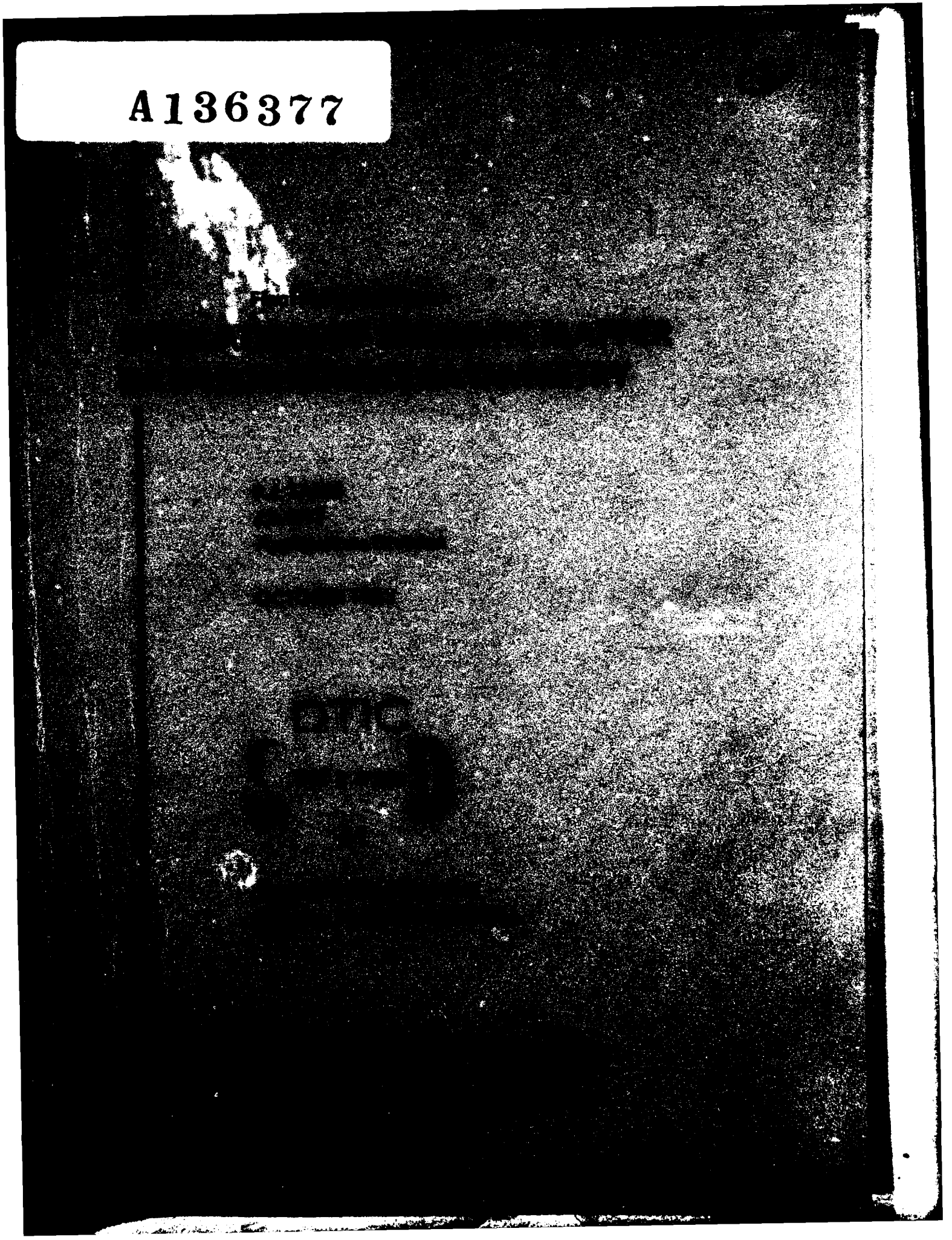

TECHNICAL REPORT STANDARD TITLE PAGE

1. Report No.	2. Government Accession No.	3. Recipient's Catalog No.
163100-7-F	AD-A136377	

4. Title and Subtitle	5. Report Date
SIMULATION OF THEMATIC MAPPER DATA FOR REMOTE BATHYMETRY	OCTOBER 1983
	6. Performing Organization Code

7. Author(s)	8. Performing Organization Report No.
F.J. Tanis and J.S. Ott	163100-7-F

9. Performing Organization Name and Address	10. Work Unit No.
Environmental Research Institute of Michigan Applications Division, P.O. Box 8618 Ann Arbor, Michigan 48107	11. Contract or Grant No. N00014-82-C-2311

12. Sponsoring Agency Name and Address	13. Type of Report and Period Covered
Naval Research Laboratory 4555 Overlook Avenue, SW Washington, DC 20375	Final Technical Report
	14. Sponsoring Agency Code

15. Supplementary Notes

16. Abstract

A preliminary algorithm has been developed for the extraction of water depths from Thematic Mapper (TM) scanner data. Algorithm development was based on 1978 aircraft scanner (ERIM M-8) data processed to simulate TM data, and on data available from the 1980 Photobathymetric Calibration Survey. The Defense Mapping Agency (DMA) constructed a series of overlays to the ERIM data set showing locations of ship soundings. These overlays were used as a basis to extract corresponding TM simulated signals from the aircraft data set. Water depth prediction algorithms were developed based upon relationships between the simulated TM data and the measured water depths. Results will aid the development of bathymetric processing procedures for Thematic Mapper data.

17. Key Words	18. Distribution Statement
Thematic Mapper Bathymetry Water Depth Remote Sensing	

19. Security Classif. (of this report)	20. Security Classif. (of this page)	21. No. of Pages	22. Price
Unclassified	Unclassified	v + 63	

PREFACE

This final report was prepared by the Applications Division of the Environmental Research Institute of Michigan (ERIM) under Naval Research Laboratory (NRL) contract N00014-82-C-2311 and covers the work performed from July 20, 1982 through April 20, 1983. The technical representative for the contracting officer was Peter A. Mitchell of NRL. The principal investigator was Fred J. Tanis with important contributions to the technical program made by Jaci Ott and Tom Wessling. This technical work was conducted by the Applications Division under the direction of Mr. Donald S. Lowe.

This contract involves the development of preliminary water depth extraction algorithms for use with Thematic Mapper Scanner (TM) data. The techniques and processing procedures developed under this contract were based on a set simulated TM data derived from aircraft multispectral scanner data collected previously over the Bahamas Photobathymetric study area.

TABLE OF CONTENTS

LIST OF FIGURES

LIST OF TABLES

1.0

SUMMARY

The recent launch of Landsat-D with its Thematic Mapper Sensor (TM) represents an excellent opportunity for the Defense Mapping Agency (DMA) to improve its passive satellite remote bathymetry capability. DMA provided inputs to the selection of spectral bands for the TM sensor. It is anticipated that the refined spectral and spatial resolutions will greatly improve the possibilities for extraction of accurate water depths from remote sensing data. DMA has supported the development of a set of preliminary algorithms based on TM data simulated from airborne surveys to help prepare for the eventual extraction processing with TM data. This effort compares results obtained from aircraft data at one and ten meter resolutions with that obtainable from simulated TM spatial resolutions (30 m). These data sets will provide a valuable calibration source for actual TM data collected over the same area.

ERIM M-8 multispectral scanner data collected during August 1978 over the Bahamas Calibration Area have been used to both spectrally and spatially simulate the Thematic Mapper data. The spectral simulation was accomplished by summing narrow bands from the M-8 data set where the summing weights were determined from band response functions for both sensors. Spatial simulation was achieved by window averaging the aircraft data set to thirty meters resolution from either one or ten meters nadir resolution. Simulation of the radiometric properties of TM data was not practical in the present study because (1) TM absolute radiometry is not well understood, (2) the large differences in collection platform altitude, and (3) difficulties in absolute radiometric calibration of the aircraft scanner. However, these aircraft data provided a means to examine predicted water depth as a function of spectral or spatial resolution.

Ship survey soundings and subsurface radiometric measurements collected by Science Applications, Inc. (SAI) during the July 1980 survey

were used for surface truth. A series of image to photo map registration processes were required to merge these survey data with the TM simulated data. The airborne scanner data were corrected for scan angle distortions and resampled to one and ten meter pixel sizes. DMA used an analog process to rectify a cartographic plot of the ship sounding locations to an image of the TM simulated data. An overlay was produced showing precise location of the soundings. This overlay was digitized at ERIM and used to extract the desired set of simulated TM responses at each sounding location. These data were then assembled with the measured water depth and subsurface photometer readings. The assembled calibration data set served as a basis for preliminary algorithm development and error analysis with respect to bottom reflectance changes.

Three types of algorithms were examined for each of two apparent bottom types (1) sand and (2) mixed sand with vegetation. The calibration data set consisted of a total of thirteen ship transects, which were partitioned into a subset for algorithm derivation and one for algorithm verification. Algorithm types considered included three band regression, two band regression, and two band ratio. The results from these analyses defined the best algorithm as a two band (TM1, TM2) regression algorithm. An effective three band regression algorithm could not be developed since TM band 3 (0.63-0.69 microns) has very little penetration to the majority of the water depths contained in the calibration set.

For this study the three band regression algorithm yielded predicted depths in shallow areas (<5m) which were within a few tenths of a meter for most pixels of those from the two band regression algorithms. Since the third band did not penetrate effectively to the bottom for many of the pixels in the study area, it did not produce a predicted depth for many of the pixels. For many of these pixels the simulated TM3 signal was less than that determined for the deep water. Although

it could not be demonstrated with the M-8 data set, a three band regression algorithm could be developed for these waters. It would likely produce more accurate predictions for depths of up to five meters, beyond which a two band regression algorithm could be applied.

The ratio algorithm (TM1/TM2) produced results comparable to that of the two band regression algorithm when the K values were computed from the calibration data set over a sand bottom. The ratio prediction was found to be more sensitive to bottom vegetation changes at 8 to 10 meters depth and to have more noisy predictions for deep waters of the scene (>20m) than those obtained with the two band regression algorithm.

Spatial resolutions considered in this study included one, ten, and thirty meters. Results using the two band regression algorithm for each of these resolutions showed that the depth calculations from data with higher resolutions had higher levels of environmental noise. This noise is defined as the combination of fluctuations in the surface reflected signal and the atmospheric path radiance that remains after a correction is made for sun glint. This noise source is separate from that due to electronic "system" noise. The bottom cover type was found to influence the water depths predicted with the two band regression algorithms, especially with the one and ten meter resolution data. From shallow to deep water the observed depth errors (4-10 m depths) first diminish due to decreased sensitivity to bottom reflectance then increase (>15 m depth) as the influence of environmental and system noise becomes more prominent. Thus, the midrange water depths (10-15 m) can be expected to show minimum depth errors. In addition, depth prediction errors due to bottom cover features were greatly reduced in the thirty meter pixel depth chart. For the Cat Cay calibration area it appears that the TM spatial resolution would produce water depth charts which are less influenced by bottom reflectance changes than those charts which could be obtained using a higher spatial resolution. Thus, given an equivalent environmental noise condition, the TM data would be expected to

produce more accurate depths than those produced at aircraft resolutions. Evidence to date would suggest, outside of the problem of spatial variability of haze (aerosols), that environmental noise is greater for higher spatial resolutions due principally to surface effects. Thus, the use of higher resolutions may be only warranted in cases where it is necessary to detect and chart a rapidly changing water depth (point hazard).

A series of transparent overlay products were developed for the DMA base photo map. These overlays consisted of grey tone depth charts, where each pixel was processed to (1) estimate a water depth, and (2) derive plots of actual predicted depth values in smooth sheet format. These overlays facilitated interpretation of algorithm behavior over a variety of bottom features and at multiple resolutions.

The present study has helped to improve our understanding of the potentials of extracting water depths from TM data. Preliminary multiple band water depth algorithms have been developed for TM data. However, these algorithms rely heavily on the availability of ship calibration information. The goal at DMA is to develop algorithms which can be applied to TM data over a range of environmental viewing conditions without the requirement for ship calibration data. In order to develop such data dependent algorithms, it will require working with actual, rather than simulated, TM data where one can model the influence of various parameters on the value of the regression coefficients in the present extraction algorithms.

2.0

INTRODUCTION

The need for a reliable capability to extract hydrographic information from passive remotely sensed data has greatly increased as conventional depth surveys by hydrographic vessels have not been able to keep up with the demand. DMA has increased its effort to develop a satellite/airborne remote sensing survey capability which would allow charts to be updated in a more efficient manner. Algorithm development for satellite remote bathymetry has been supported by the Defense Mapping Agency (DMA) and the Office of Naval Research (ONR) in several projects [1,2,3]. Emphasis has centered on satellite studies which have utilized the Landsat Multispectral Scanner (MSS) green band (MSS-4) and red band (MSS-5) to map the more extensive areas of the world which receive satellite coverage. The use of the MSS is limited, except for shallow waters, to a single band (i.e., MSS-4). Because of the increased spectral and spatial resolution airborne active passive multi-band techniques have been shown to be far superior to satellite techniques [1]. The launch of Landsat-D in July 1982 offered an opportunity to develop new and improved satellite algorithms to chart the shallow waters using the Thematic Mapper (TM) Scanner. The availability of three TM bands, one of which is ideally located for shallow water penetration, plus the improved radiometric sensitivity is expected to result in greater depth mapping accuracy and the ability to extract greater water depths. In addition, there is a better than 2X improvement in the sensor spatial resolution as compared to MSS. Early TM imagery shows remarkable detail in the water in the blue-green and yellow bands. The multiple bands will potentially allow the use of more sophisticated algorithms which minimize interference from bottom type, water clarity, sun glint, and haze.

In order to help evaluate this potential, DMA has supported the present study to design preliminary bathymetry algorithms for TM data based upon available aircraft multispectral scanner data.

2.1 BACKGROUND

During the summer of 1978, a series of data collection flights were conducted at the request of DMA in conjunction with their measurement program creating the Bahamas Photobathymetric Calibration Area. Extensive ship surveys were made at this time based on a DECCA navigation grid. The ERIM M-8 active/passive scanner system was used to collect both nadir laser pulse data (LIDAR) and passive multispectral scanner data. Flights were made over five test areas at 1,000 feet and 10,800 feet altitude. These data were analyzed in a previous study for the Naval Coastal Systems Laboratory where the laser data were used to calibrate the passive bathymetry depth algorithms [3]. Algorithms considered were either two band regression type or two band ratio type and were processed under three separate conditions: (1) calibration with laser depths, (2) calibration with ship depths, and (3) no calibration. Of these processings, the one using the laser depths for calibration was found to produce the most accurate predictions. Laser depths were found to be known more accurately within the data set, in comparison with the ship data because of difficulties and inherent inaccuracies with the DECCA navigational system [3].

During the summer of 1980, as part of a continuing program to establish the Calibration Area, DMA sponsored a broad set of experiments and survey measurements [4]. These experiments were designed to acquire a valid and comprehensive set of bathymetric and photometric data. The purpose was not only to establish position and depth information needed to calibrate water depth measurements made by multispectral sensors on spacecraft and aircraft, but also to measure the spectral characteristics of bottom algae and coral reef communities [5].

The survey vessel was fitted with a submersible photometer with spectral bands corresponding to TM bands one through three. This photometer was designed and calibrated by the Johns Hopkins Applied Physics Laboratory (APL) and is subsequently referred to as the APL photometer.

The basic measurement made with the photometer system is the effective bottom reflectance for each of the bands sampled. The effective reflectivity was defined to be equal to the ratio of the voltage level from the photometer to that of a KAHL cell located on deck and multiplied by a calibration factor based on known reflectance values of a calibration panel [4]. Other data collected included spectral scans of bottom samples [6], light extinction coefficient determinations, and ocean bottom photography.

2.2 STUDY OBJECTIVES

The present study had four principal objectives. (1) Develop preliminary algorithms for TM data and evaluate and define the principal errors in each algorithm using the supporting calibration survey results obtained from objectives (2) and (3). (2) Process the M-8 scanner data sets of the Bahamas Photobathymetric Calibration Area to simulate the spectral and spatial properties of the Thematic Mapper bands. (3) Merge the 1980 survey depth and APL photometer data into calibration data sets. (4) Prepare grey level depth charts for each algorithm and transparent overlays showing numerical depths over a variety of bathymetric features.

3.0

PREPARATION OF TM SIMULATED DATA SETS

3.1 DESCRIPTION OF THE AIRCRAFT DATA SETS

The sets of aircraft multispectral scanner data used for this TM simulation study come from the Bahamas experiment conducted during July and August 1978. During that experiment, data were collected over both the Great and Little Bahama Banks at flight altitudes of 1,000 and 10,800 feet. The low altitude flights included collection of both active and passive data. Lidar calibrations of these passive data have been made in a previous study [3]. The passive data were collected in eight spectral bands which encompass the first four TM bands (see Table 1).

TABLE 1

SPECTRAL BANDS FOR THE ERIM M-8 SCANNER

DATA CHANNEL	WAVELENGTH (μm)
C2	.67-.94
C4	.62-.67
C5	.58-.64
C6	.55-.60
C7	.52-.57
C8	.50-.54
C9	.48-.52
A1	8.2-14.0

For this study seven of the M-8 data flights were selected for TM simulation. These runs provided both high and low altitude coverage for Bimini, Cat Cay, and Great Issac Photobathymetric Calibration Areas. In addition, a high altitude run for the Rocky Heads area was selected for simulation (see Table 2 and Figure 1). Site and run selection were based upon the DMA interest in the specific area, data quality, and coincident Aerial Survey International (ASI) color photography.

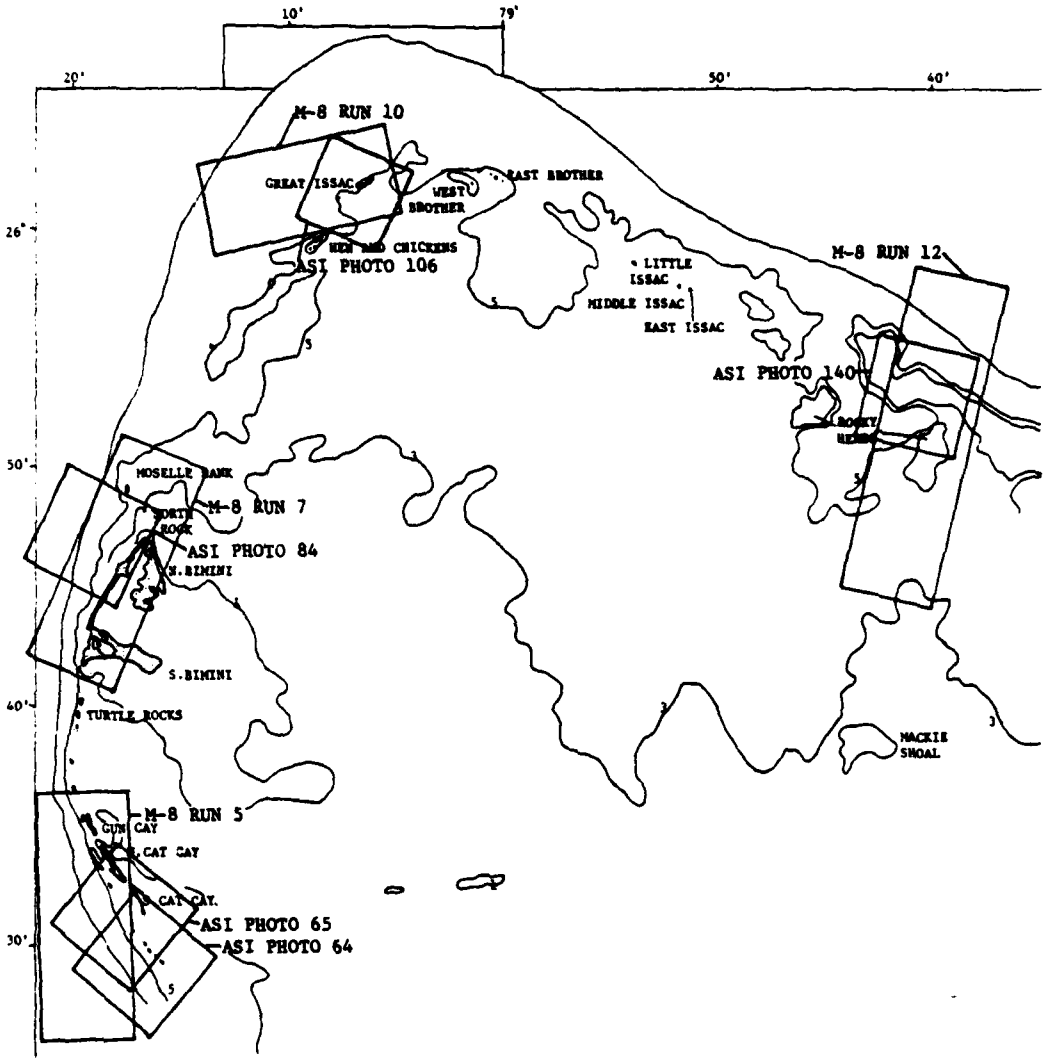

FIGURE 1. LOCATION OF TM STUDY AREAS

TABLE 2

SUBAREA DATA SETS

STUDY AREA	M-8 RUN*	TIME	ALTITUDE (ft.)	ASI FRAME NO.**
North Cat Cay	2	0900	1,000	0064
North Cat Cay	5	0900	10,800	0064,0065
Bimini	7	1600	1,000	0084
Bimini	7	1600	10,800	0084
Great Isaac	2	1600	1,000	0105
Great Isaac	10	1600	10,800	0105
Rocky Heads	12	1600	10,800	0140

* Collected 12 August 1978
**Collected January 1981

Eight individual aerial photo frames were identified to be used as a geographical reference base for this study. The coverage in each of these photo frames included ship survey transects where water depth and photometer data were collected during the 1980 calibration survey experiments. The bottom features for each of these study areas are expected to be highly stable and not subject to significant changes over the time period separating photo and M-8 data collections.

3.2 CREATION OF THIRTY METER RESOLUTION DATA SETS

The thirty meter TM spatial resolution was simulated by window averaging either the one or ten meter data sets. For example, the thirty meter resolution was estimated from the ten meter data by averaging nine ten meter by ten meter pixels and replacing each of those nine values with the average result. The window was then positioned on a new set of pixels and the process repeated. The resulting thirty meter simulation data set contains the same number of pixels as the input ten meter set so that the two sets could be used to produce transparencies or overlays to the same scale. The window averaging process

was used to degrade the high altitude ten meter data to thirty meters resolution and the low altitude one meter data to ten and thirty meters resolution.

Over portions of the scene with nearly constant depth or bottom reflectance, the averaging process will produce a product which is less noisy. Over areas of rapidly changing bottom (depth, vegetation, or both) the averaged data set will be less sensitive to bottom reflectance.

3.3 SPECTRAL SIMULATION FOR TM

The M-8 scanner spectral bands cover the TM bands and, therefore, spectral simulation can be achieved by combining appropriate M-8 bands. Based on published TM response curves for TM bands 1 through 4 and those measured by the M-8 scanner, a series of band coefficients have been derived for use in the simulation. An examination of these spectral response curves has shown that the following M-8 bands could be used to approximate TM spectral response (see Figure 2).

TM1: C9, C10
TM2: C6, C7
TM3: C4
TM4: C2

Weighting coefficients were derived for TM1 and TM2 although they could be applied only in the case of TM2 since C10 was not available for the flightlines listed in Table 2. Thus, TM1 was simulated with M-8 band C9 alone. The impact of the loss of the C10 channel on the present study is difficult to assess. However, the response curves shown in Figure 2 would suggest that some loss in penetration depth was sustained with these simulation data sets, because the blue-green portion of TM-1 sensitivity was not simulated. In the case of TM2 the weighting coefficients were obtained by least squares solution of

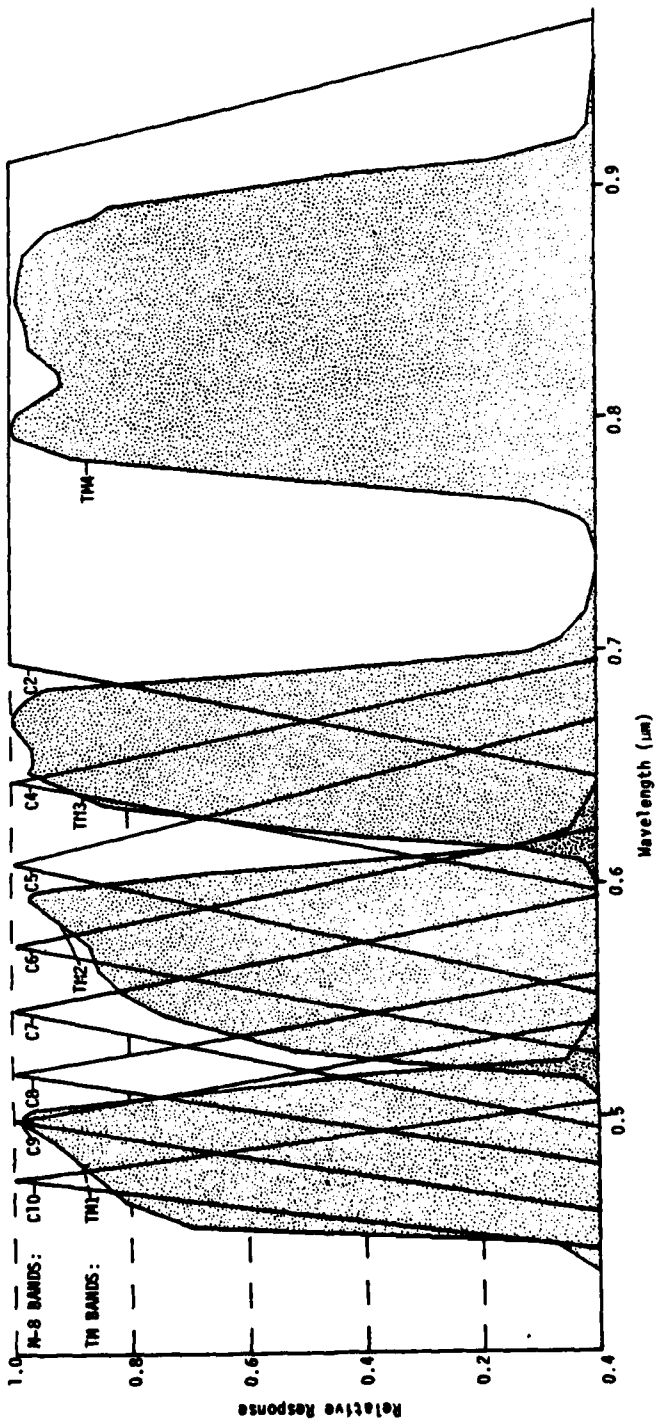

FIGURE 2. COMPARISON OF TM AND M-8 SCANNER SPECTRAL BANDS

$$TM2(\lambda) = a_1 \cdot C6(\lambda) + a_2 \cdot C7(\lambda)$$

where response points were taken at 5nm intervals across the entire response range of TM2. This analysis resulted in values of a_1 and a_2 of 0.3137 and 1.0264, respectively. For TM1 the weighting coefficients obtained were 0.8010 and 0.7885 for M-8 bands C9 and C10. In the case of TM2 these coefficients were further adjusted to account for M-8 gain settings, calibration lamp values, and blackbody radiance values which can vary with individual flights runs (see Table 3). The calibration lamp had been previously measured with a radiometer for each lamp current setting. Thus the radiance L(m) in a particular M-8 band m can be calculated as:

$$L(m) = \frac{SL(m) - BB(m)}{LAMP(m)-BB(m)} \cdot \frac{L(n\text{-}AMPS, m)}{DETECTOR\ GAIN\ (m)}$$

where SL(m) is the signal level count in M-8 band m, BB(m) is the blackbody count, LAMP(m) is the lamp count, and L(n-AMPS, m) is the lamp radiance as seen by detector m for the current of n amps. Lamp and blackbody counts are reported in Table 3 and were taken as peak values in the scan line and averaged over several scan lines in each run to obtain a good estimate. Subsequently, the radiance values at each pixel for M-8 bands C6 and C7 were multiplied by the weighting coefficients and summed to obtain the corresponding radiance in TM2. These latter TM2 radiances were then scaled to eight bit signal counts (0-255) based upon maximum run signals in C6 and C7.

TABLE 3

M-8 CALIBRATION VALUES

	Bimini 1,000'	Bimini 10,800'	Cat Cay 1,000'	Cat Cay 10,800'	Great Issac 1,000'	Great Issac 10,800'	Rocky Heads 10,800'
Blackbody							
C6	12	2	0	0	11	3	15
C7	0	0	0	0	20	3	18
Lamp Cal.							
C6	90	56	5	2.5	165	52	153
C7	24	40	2	1	80	34	73
Lamp Radiance							
C6	3.7	3.7	.950	.950	2.4	.950	2.4
C7	3.5	3.5	.800	.800	2.1	.800	2.1
Current	4.8	4.8	4.0	4.0	4.5	4.0	4.5

This spectral simulation resulted in a four channel data set which best simulates the first four TM bands using the available M-8 aircraft scanner data. No attempt was made to radiometrically simulate the TM data with this aircraft data set because of differences in sensor platform altitude, scan geometry, and noise characteristics.

3.4 IMAGE WARPING PROCESSING

Eight ASI aerial photos, as listed in Table 2, were chosen for the geographic reference base for the present study as based on features of interest and coincidence with the remote sensing data. The seven TM simulated data sets were image warped to fit the respective photographs as accurately as possible. It was not possible to define a standard mapping projection or geographic coordinate system for the photographs.

Initially, efforts were made to apply the ERIM spacecraft image warping software to these aircraft data. This approach is not a routine operation and numerous software modifications were tested to improve the accuracy of the procedure. The image warping polynomials contain

sufficient higher order terms that are not valid beyond the immediate area of suitable ground control points. Most of the TM simulated data sets contain large open water areas of sufficient depth to mask features that might be used for control. The spacecraft software, therefore, produced unacceptably distorted results.

The affine transformation was evaluated and found to be sufficiently accurate for these data sets. Scan angle effects that might have limited the performance of the warping process were corrected. Table 4 contains the standard errors (S.E.) of the control points for each of the TM image transformations. Errors are shown both in terms of input pixel and in meters.

TABLE 4

STANDARD ERRORS FOR
AFFINE IMAGE TRANSFORMATIONS

TM DATA SET	ALTITUDE (FEET)	NO.OF CONTROL POINTS	VERTICAL PIXEL S.E.	HORIZONTAL PIXEL S.E.	INPUT PIXEL (M)	VERTICAL S.E. (M)	HORIZONTAL S.E. (M)
Cat Cay	1,000	13	3.8	4.2	0.76	2.9	3.2
Bimini	1,000	11	3.8	6.2	0.76	2.9	4.7
Bimini	10,800	9	3.0	2.0	8.23	24.6	16.8
Great Issac	1,000	18	8.5	3.0	0.76	6.4	2.3
Great Issac	10,800	12	3.0	1.3	8.23	24.6	10.8
Rocky Heads	10,800	8	3.4	3.1	8.23	27.6	25.1
Cat Cay	10,800	16	3.5	3.7	8.23	28.8	30.1
Cat Cay	10,800	20	6.0	3.0	8.23	49.0	24.5

Also shown is the number of control points used in each case. Control points were selected as readily identifiable features in both images with sharp contrast boundaries and, to the extent possible, to be evenly distributed over the entire scene.

The number of control points required to implement the image warping software beyond the minimum needed to obtain a solution is not specified by the software and remains a matter for judgement. Selection of control was considered by the analyst to be complete for each image. In each case it was felt that selection of additional control points would be either of poorer quality or have redundant location and would therefore, not enhance results from the image warping algorithm.

To test the importance of the number of control points the Cat Cay (10,800') image warp to ASI photo 64 (January 3, 1981) was repeated using 7, 10, 12, and 16 control points. The horizontal and vertical standard errors were found to drop dramatically as the number of control points was reduced. Thus error reduction was expected since the regression equation has fewer points to fit. The resultant quality of the resampled image was the best indicator of the effect of number of control points on image warping. In general the fit of the resampled scenelet is good in some areas and poor in others. However, the difference in quality of fit due solely to the number of image control points available appears to be minor.

The portion of the TM simulated data sets coincident with ASI photos was then warped with the affine transformation to fit as accurately as possible. The low altitude data were resampled to one meter output pixels and the high altitude to ten meters. Transparent overlays of TM simulated band 1 were produced and forwarded to DMA for purposes of annotation of 1980 survey soundings.

3.5 INTEGRATION OF SHIP SURVEY MEASUREMENTS

Ship survey transects were photographically rectified at DMA to the previously constructed simulated TM image. These latter images, as discussed above, had been warped to ASI photographs of the area. Transparent overlays to the TM simulated images showing location and value for each ship sounding were constructed by DMA and provided to ERIM (see Figure 3). Due to the time and labor needed to construct accurate overlays of this type, only the Cat Cay area overlays could be completed at

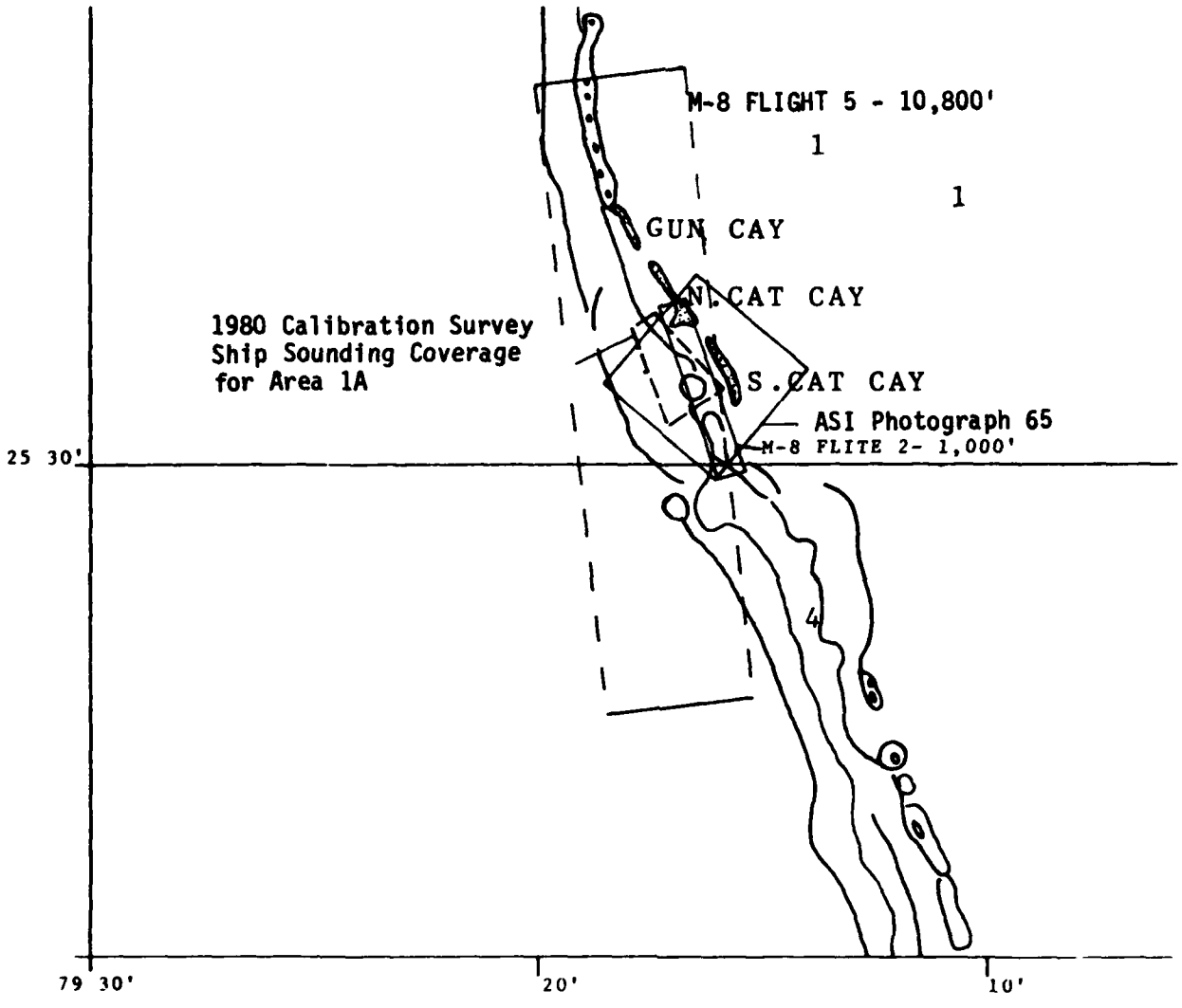

FIGURE 3. CAT CAY TM STUDY AREA

DMA within the time constraints of the program. The methodology used at DMA was to first approximate the location of the transect information in the image using reported locations of the ship soundings together with geographical coordinates of stationary control points. Refined positioning of the transects within the ERIM TM images was accomplished by fitting APL photometer transects to the observed positions of bottom reflectance changes. The same procedure was applied to both the high and low altitude imagery of the Cat Cay study area. DMA reported expected errors in the constructed overlays of two pixels (20m) for the high altitude overlay and five pixels (5m) for the low altitude data set. The high altitude overlay contained a total of 554 data points while the low altitude overlay, covering a much smaller area contained only 131 points. Portions of the overlay transects were found to be located in areas of severe sun glint which, because of saturation of either blue-green or near infrared signals, could not be totally removed by preprocessing.

3.6 EXTRACTION OF TM SIMULATED DATA

The ship transect soundings were digitized from the DMA prepared overlay using the ERIM coordinate digitizer to produce a file of image relative coordinates. Line, point coordinate locations in the simulated TM image were determined using the coordinate file and a map projection function with scales derived from the ASI photographs. Simulated signal counts for TM bands one through four were extracted from the digital image file at each transect position using available training set software. Measured depths were also entered into the coordinate file and transferred to the extracted file. Thus, the resulting calibration data file contained to the best approximation the measured water depths and corresponding simulated TM values. This file was then merged with a second file containing APL photometer measurements for TM bands 1 and 2 along with a second set of measured water depths. These latter data were taken from a listing provided by DMA. The measured values of depth

provided a basis to align the transect values from each file. Separate data sets were produced for the high altitude 10 and 30 meter resolutions and the low altitude 1 meter resolution. These assembled data sets were then used to develop and evaluate several water depth algorithms for the simulated TM data as discussed under Section 4.0.

3.7 REDUCTION OF THE APL PHOTOMETER DATA

Subsurface upwelling radiance measurements were collected along with the water depth soundings during the 1980 survey of the Bahamas Photobathymetric Calibration Area. These measurements were made using a hull mounted photometer pointed downward and located free of the bow wake turbulence. The photometer samples were electronically delayed to provide precise registration with those from the depth sounder. The photometer was designed by the John Hopkins Applied Physics Laboratory (APL) with detectors matched to the first two TM bands and a red band centered at 0.7 μm. These radiance measurements contain contributions from backscatter within the water column and by reflection from the sea bottom material. The TM3 band produced little or no useful information once it was corrected for changes in surface downwelling irradiance. This result would suggest that TM3 (as implemented in the APL photometer) has insufficient penetration over these survey water depths of 4 to 15 meters. In each of the other two bands the measured radiance is largely dependent upon bottom reflectance for shallow waters (<10 m) and completely dependent upon the backscattered term at some greater depth. The smallest photometer readings in each band (very deep water or very low bottom reflectance) can be used to estimate the backscattered term. Using this value and the Jerlov values for irradiance attenuation (for Jerlov water type 1a) [7], we can estimate a term which is directly proportional to the bottom reflectance. These bottom reflectance estimates were made using the APL photometer measurements in bands 1 and 2 for a representative set of transects. Values were expressed as a ratio with the overall mean value. These calculated "reflectances"

served two purposes: (1) to allow possible identification of bottom reflectance variations as a water depth algorithm error source; and (2) as a basis to modify the algorithm estimates such that they might become independent of bottom reflectance.

3.8 CORRECTION FOR SUN GLINT

Because of the large scan angle, sun glint can cause severe radiometric distortion in aircraft data. Sun glint effects were evaluated using a previously developed statistical analysis procedure for deep water signals [3]. The technique involves examination of the correlation between the penetrating and non-penetrating bands of TM. If the correlation is low, the sun glint is considered to be low. If, on the other hand, the correlation coefficient is larger than 0.9, sun glint is significant. The correction procedure is based upon the covariance between visible and near infrared signals. The infrared signals are caused mainly by sun glint and possibly atmospheric path radiance. The correction is given by the following set of equations.

$$\Delta V_i = A_{ij} + B_{ij} V_j$$

$$A_{ij} = \bar{V}_i - (\sigma_{ij}/\sigma_{jj})\bar{V}_j$$

$$B_{ij} = \sigma_{ij}/\sigma_{jj}$$

where V_j is the signal in channel j; $\bar{V}_i$ is the average deep water signal in channel i for a totally glint free area of deep water, and σ_{ij} is the signal covariance. The ΔV_i is calculated for each pixel and substracted from the TM simulated signal.

This sun glint procedure was applied to correct both the high and low altitude data set for the Cat Cay area. The correlation and covariance values are reported in Table 5 and indicate the severity of the

TABLE 5

SUN GLINT PARAMETERS

Correlation Coefficients with TM4:

Band	High Altitude	Low Altitude
TM1:	.936	.876
TM2:	.978	.946
TM3:	.980	.978

Covariance Parameters

	σ_{ij}	B_{ij}
High Altitude:		
TM1	544.22	0.282
TM2	442.18	0.229
TM3	1048.80	0.544
TM4	1928.40	0.0
Low Altitude:		
TM1	1150.30	0.316
TM2	362.13	0.099
TM3	208.32	0.572
TM4	3642.7	0.0

glint problem. Deep water signal levels before and after correction are compared in Table 6. The signal variance was reduced by more than half in most cases for these data sets.

For the high altitude data set the mean signal level after correction agrees well with those mean values reported for a glint free area of deep water. In the case of the low altitude data the same statistics indicate that some of the noise and signal level due to sun glint remain after applying the correction procedure. It is likely that portions of these data sets had near saturated signal levels which are not suitable for this correction procedure.

In general the low altitude data set was found to be noisy even after correction as indicated by the relative size of the standard deviation values in Table 6. Furthermore, there was sufficient remaining noise to severely degrade the performance of any subsequent depth processing.

Sun glint corrected images for the Cat Cay area at both 10 and 30 meter resolution are shown in Figures 4, 5, and 6 for TM bands 1, 2, and 3, respectively. The corresponding low altitude data sets are shown in Figure 7.

TABLE 6

COMPARISON OF DEEP WATER SIGNAL STATISTICS

Variable Sun Glint Area

	Before Correction		After Correction	
	Mean	Std. Dev.	Mean	Std. Dev.
High Altitude				
TM1	118.49	15.19	103.03	5.07
TM2	57.42	11.90	44.86	2.60
TM3	93.19	28.17	63.38	5.87
TM4	133.75	43.91	133.75	43.91
Low Altitude				
TM1	143.66	30.59	112.64	16.44
TM2	30.43	11.06	20.08	5.69
TM3	73.96	50.52	21.71	5.87
TM4	100.92	60.55	100.92	60.55

Area Unaffected by Sun Glint

	Mean	Std. Dev.
High Altitude		
TM1	105.97	3.92
TM2	45.80	1.46
TM3	63.10	2.92
TM4	83.21	5.44
Low Altitude		
TM1	68.26	10.21
TM2	12.18	3.13
TM3	16.17	13.35
TM4	12.75	3.78

10 M Resolution

30 M Resolution

FIGURE 4. TM BAND 1 IMAGERY FOR CAT CAY AREA WITH TEN AND THIRTY METER RESOLUTION AS SIMULATED FROM M-8 SCANNER DATA, RUN 5, 12 AUGUST 1978

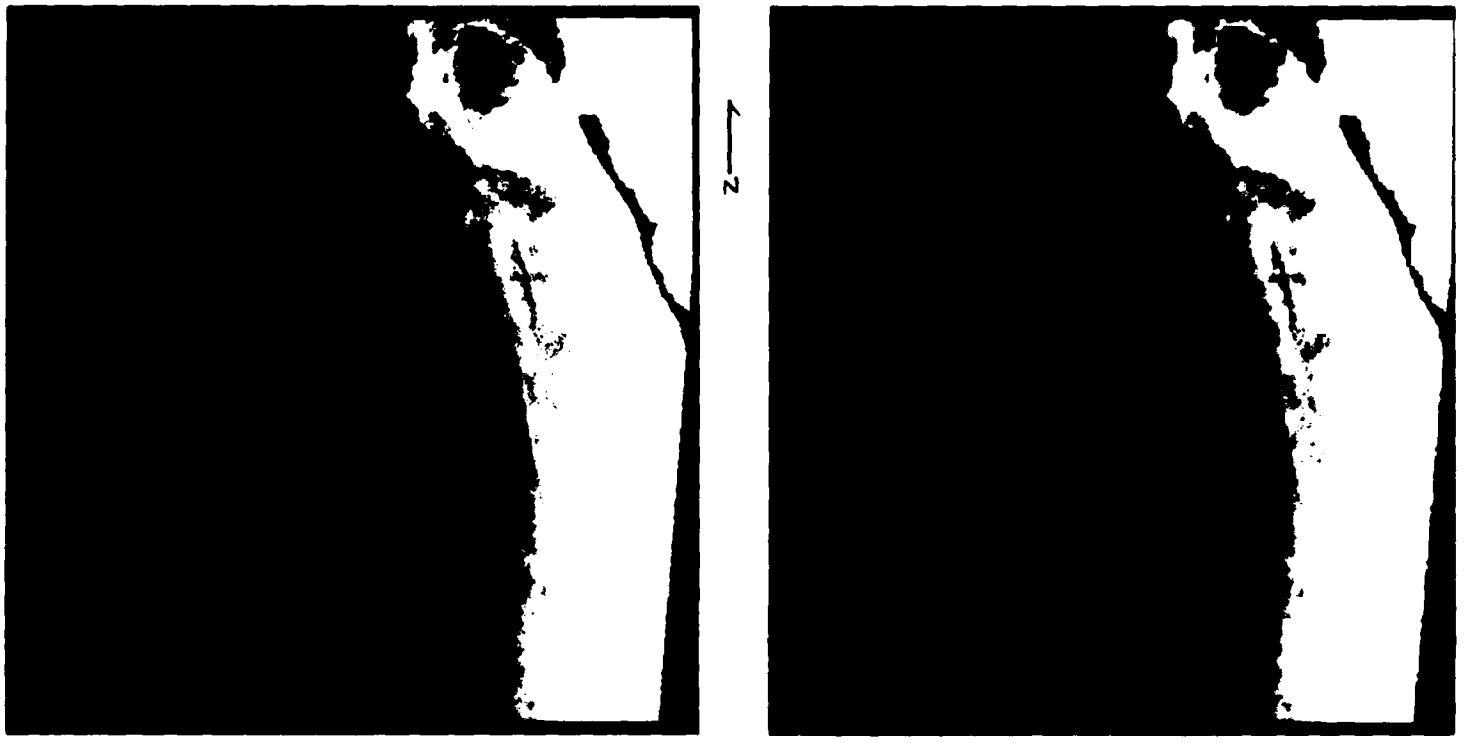

10 M Resolution

30 M Resolution

FIGURE 5. TM BAND 2 IMAGERY FOR CAT CAY AREA WITH TEN AND THIRTY METER RESOLUTION AS SIMULATED FROM M-8 SCANNER DATA, RUN 5, 12 AUGUST 1978

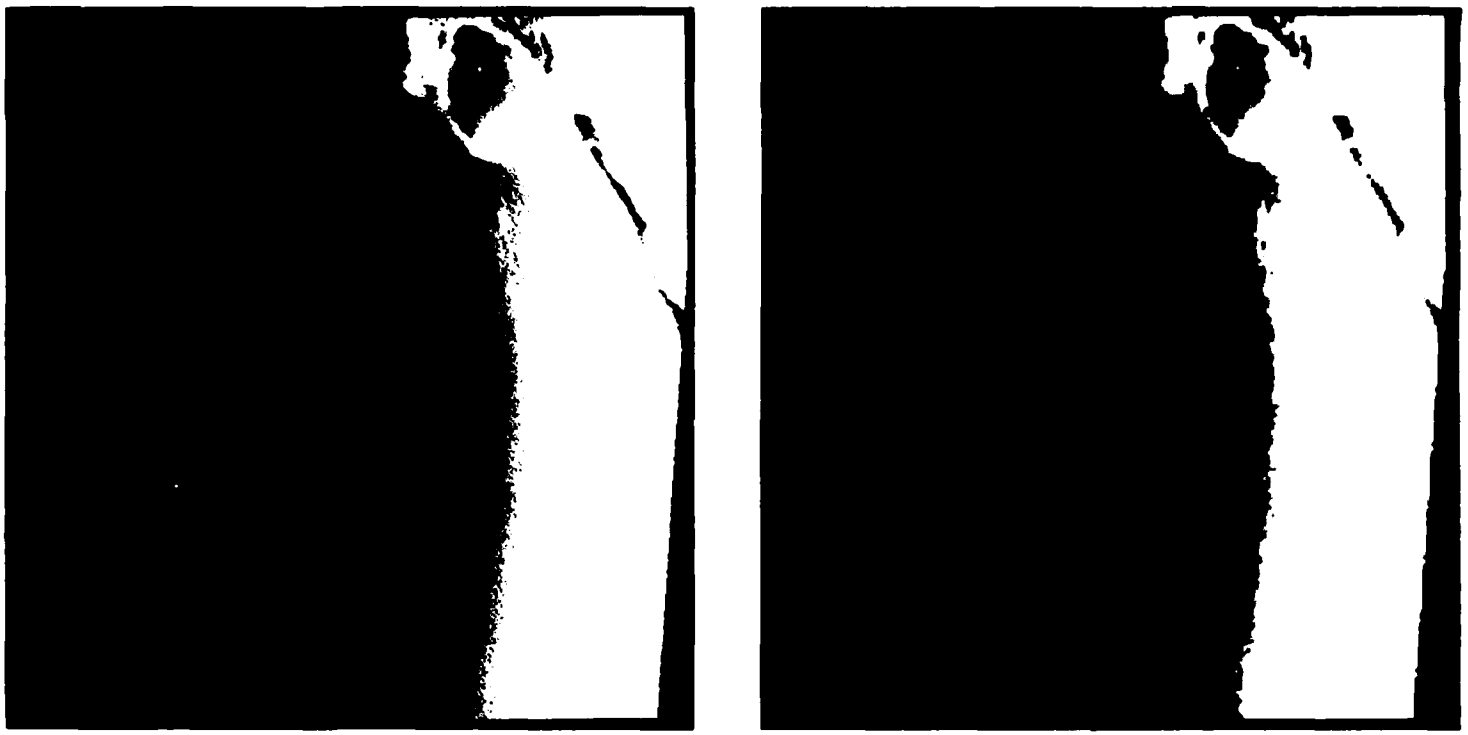

10 M Resolution

30 M Resolution

FIGURE 6. TM BAND 3 IMAGERY FOR CAT CAY AREA WITH TEN AND THIRTY METER RESOLUTION AS SIMULATED FROM M-8 SCANNER DATA, RUN 5, 12 AUGUST 1978

BAND 1

N

BAND 2

BAND 3

FIGURE 7. TM BANDS FOR CAT CAY AREA WITH ONE METER RESOLUTION AS SIMULATED FROM M8 SCANNER DATA. COLLECTED AT 1000 FT ALTITUDE ON 12 AUGUST 1978, RUN 2

4.0

DEVELOPMENT OF PRELIMINARY TM ALGORITHMS

A depth extraction algorithm for TM generally consisted of all the processing steps involved in generating a depth chart from raw data. The procedure used for actual TM data will involve a number of preprocessing steps such as geometric correction, sun glint correction, and determination of deep water signal level as were described in the previous section. In this simulation study our purpose is to show the potential performance of TM depth processing algorithms when applied to a set of data having the same spectral and spatial resolutions. While similar extraction procedures could be applied to actual TM data, radiometric difference between simulated and real TM data would imply a different set of calibrated depth equations.

The general relationship between passive signals and water depth (z) is described by the following equation.

$$z = a + \sum_{i=1}^{N} b_i \, \ell n(V_i - V_{si})$$

where the a and b's are calibration constants and V_i and V_{si} are the signal level and average deep water signal respectively in band i. The data base of ship depth soundings and extracted TM simulated signals, as described previously in section 2.2 provides a means of direct calibration of the above equation. The first step is to compute the variables $X_i = \ell n(V_i - V_{si})$ for each member of the calibration set. Standard regression techniques can then be applied to estimate values for the coefficients. This analysis results in a set of equations; each with a multiple correlation coefficient and a standard error of the predicted depth. The band pair and band triple with the highest correlation and lowest standard error can then be selected as the best two band and three band algorithm. If we consider a two band case and place the constraint on the above equation that $b = b_i = -b_j$ then the resulting equation is

equivalent to the ratio method [3]. In this case, b is related to the water attenuation coefficient K. The constant term (a) can be estimated from the shallow water signals as reported in earlier studies [1]. The ratio method produces a depth estimate which is independent of the bottom reflectance when the reflectance within the two wavelengths is proportional for all bottom types. In this study the TM simulated data were used to derive a "best" two and three band regression algorithm as well as a ratio algorithm.

The objective in developing these regression equations is to examine the relative sensitivity of the predicted water depth to environmental noise and bottom type changes under various spatial resolutions and numbers of bands for spectral definition.

As previously discussed the calibration data for the high altitude data set consisted of 554 points in thirteen ship transects as provided in the DMA overlay. The position of the transects relative to bottom reflectance changes was examined on this overlay. Transects 1, 6, 7, and 9 were selected to consist of mixed sand and vegetated bottom types. Transects 10, 11, and 12 were interpreted to primarily have a sand bottom, or at least substantially more sand than the latter grouping. Each of these groupings of transects were subsequentially used to calibrate the various algorithms. The remaining transects (1 and 2, 3, 4, 5, 6, 13) could be used in each case to examine the validity and representativeness of the calibrated algorithm.

4.1 TWO BAND REGRESSION RESULTS

Results from the two band regression analysis of 10m simulated data for TM band pairs 1 and 2, 1 and 3, and 2 and 3 are shown in Table 7 for mixed and sand bottom types. For the 10m resolution data, the correlation coefficients (between calculated and actual depths) for the TM1 and 3 and TM2 and 3 band pairs are not as high as for the TM1 and 2 band pair, indicating that the former two band pairs are not as useful as the latter band pair. This conclusion is further supported by the larger

Table 7. Results for Two Band Regression Analysis

Resolution	Bottom Type Transect Numbers	Regression Equation	Correlation Coefficient	Standard Error (M)
10 meter	Mixed, # 1, 6, 7, 9	(1) $\hat{Z} = 6.64X_1 - 11.3X_2 + 25.5$	0.948	0.868
	Sand, # 10, 11, 13	(2) $\hat{Z} = 8.27X_1 - 12.3X_2 + 21.8$	0.955	0.945
	Mixed, # 1, 6, 7, 9	(3) $\hat{Z} = -0.602X_1 - 1.41X_3 + 15.4$	0.519	2.44
	Mixed, # 1, 6, 7, 9	(4) $\hat{Z} = -6.51X_2 - 0.432X_3 + 36.8$	0.810	1.67
	Normalized with APL - Photometer	(5) $\hat{Z} = 4.24X_1 - 7.17X_2 + 20.2$	0.933	0.982
30 meter	Mixed, #1, 6, 7, 9,	(6) $\hat{Z} = 7.70X_1 - 11.7X_2 + 22.5$	0.974	0.612
	Sand, #10, 11, 13	(7) $\hat{Z} = 9.33X_1 - 12.9X_2 + 19.5$	0.978	0.661
1 meter	mixed: all sun glint free areas	(8) $\hat{Z} = 1.75X_1 - 3.81X_2 + 10.1$	0.839	1.04

Where $\hat{Z}$ is the predicted water depth (M)

X_i is $\ell n(Vi - V_{si})$ for simulated TM band i

standard errors for the TM1 and 3 and TM2 and 3 band pair algorithms, 2.44m and 1.67m respectively for the mixed bottom case, as compared with 0.945m for the TM1 and 2 band pair for the same case. Further evidence is supplied by analysis of the partial correlation coefficients (not shown). Also shown as Table 8 are results from performing separate regressions for each of the individual transects the resulting statistics indicate the variability of a two band regression analysis across the entire data set. The similarity of these individual transect coefficients suggest that a single regression equation would work reasonably well for the entire data set.

The spatial averaging process was also used to produce a similar calibration data set for the thirty meter resolution. Since each of the nine pixels were replaced with the mean value in the spatial averaging procedure, the resultant extracted set contains, as with the ten meter set, a total of 554 points. Within this set there are frequently multiple ship soundings for each TM 30m pixel which resulted in multiple measured water depths being assigned for the same signal level. In this case, the same calculated depth was associated with each of the measured depths.

Regression results for the 30 meter calibration set are also shown in Table 7. For this case the standard error of 0.612 is substantially less than that obtained for the ten meter calibration set. This reduction is largely due to the reduction of system and environmental noise as will be discussed in section 4.4.

Predicted depths from 10 and 30 m data, along with the measured depths are plotted for transects 1 and 4, and 11 and are shown respectively in Figures 8 and 9. These plots are considered to be representative of the results obtained with the two band regression algorithm. The discrepancy between measured and predicted shallow depths as shown in Figure 9 for transect 11 is likely due to bottom reflectance anomalies. Residual depths (i.e., differences between measured and

TABLE 8

TWO BAND REGRESSION EQUATIONS
DERIVED FOR INDIVIDUAL TRANSECTS*

Transect	Number of Soundings	a	b_1	b_2	Correlation Coefficient	Standard Error (m)
1	50	27.1	7.04	-12.1	.964	.689
2	40	24.8	6.63	-11.0	.971	.647
3	40	23.7	6.22	-10.3	.883	.711
4	46	34.2	4.15	-10.6	.944	.924
5	28	22.7	8.58	-12.9	.909	1.010
6	44	23.8	7.47	-11.9	.950	.821
7	49	29.3	5.53	-10.9	.958	.720
8	46	28.9	5.63	-11.1	.976	.677
9	52	22.6	6.85	-10.8	.940	1.050
10	51	23.0	7.93	-12.2	.963	.899
11	44	27.4	7.69	-13.1	.964	.872
12	35	23.4	7.99	-12.3	.913	1.290
13	29	21.6	6.74	-10.7	.927	1.000

a = constant term

b1 = coefficient of the X_1 term

b_2 = coefficient of the X_2 term

*Used ten meter resolution data.

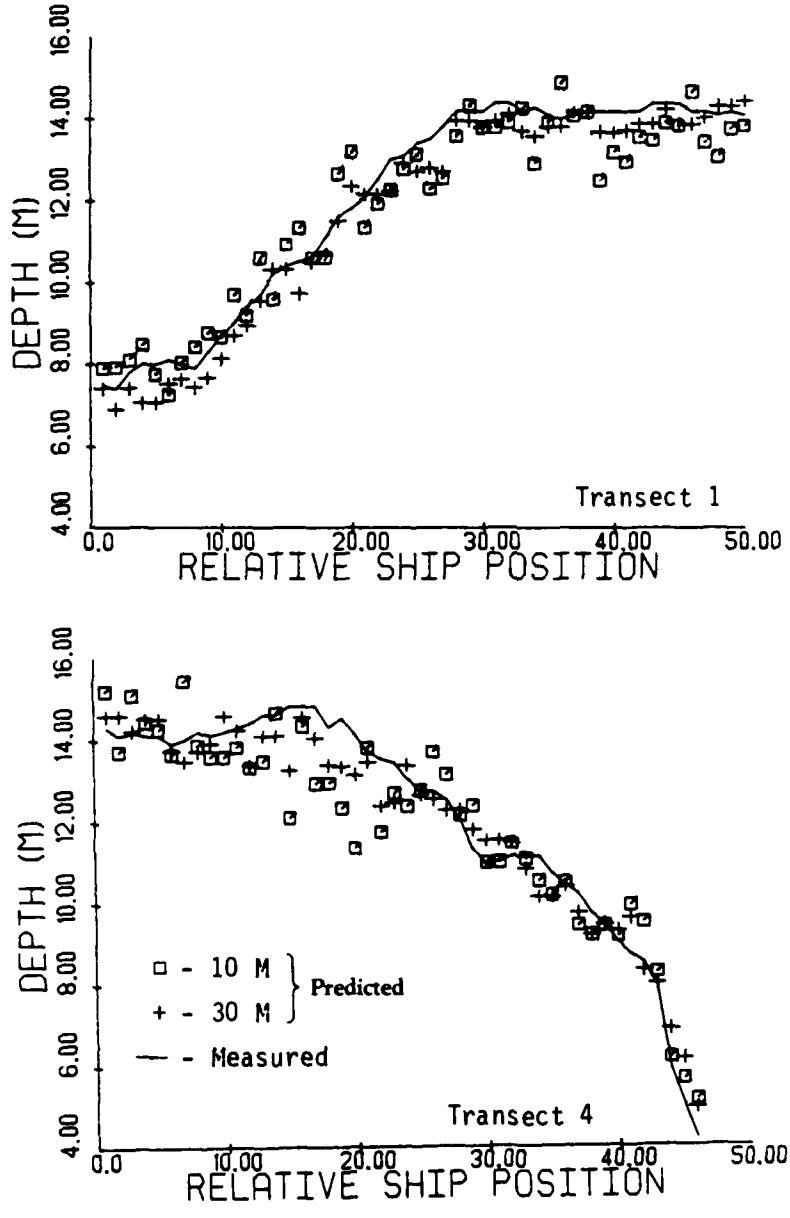

FIGURE 8. TWO BAND REGRESSION PREDICTED DEPTHS VERSUS TRANSECT POSITION FOR TRANSECTS 1 AND 4

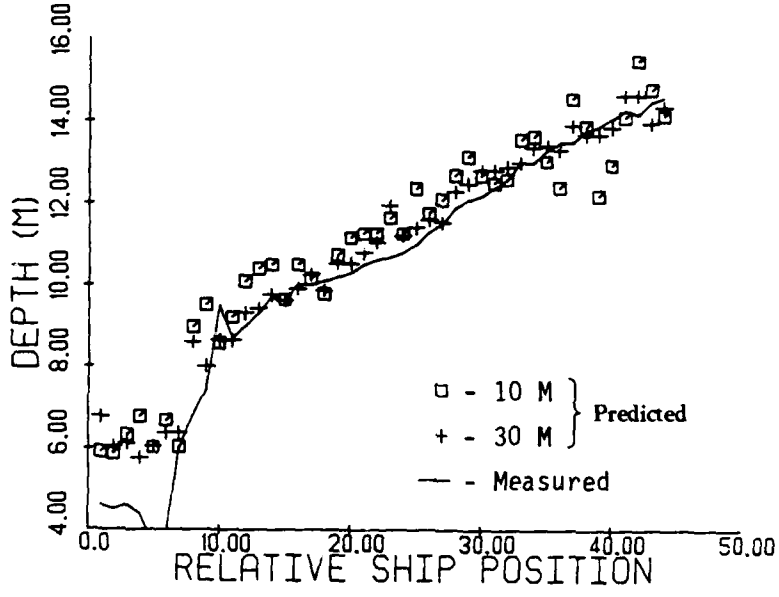

FIGURE 9. TWO BAND REGRESSION PREDICTED DEPTHS VERSUS TRANSECT POSITION FOR TRANSECT 11

calculated depth) for ten and thirty meter resolutions are shown in Figure 10 for transects 1 and 4. Also plotted in Figure 10 are the bottom reflectance indices as obtained from the APL-TM2 photometer values for transects 1 and 4 (procedure detailed in section 4.4). Here the mean reflectance has an index value of one. Transect 4 showed the greatest bottom reflectance affect on predicted depths. It is clear from the plots and others not shown, that the predicted depth at ten meters resolution is highly sensitive to these types of changes. The thirty meter residuals also display a sensitivity to bottom reflectance changes but to a much lesser degree. By contrast the results for transect 1 show little correlation between residual depth and apparent changes in bottom reflectance. These results suggest that only very large changes in bottom reflectance will have a correlated impact on the predicted depth over this calibration depth range (4-15 m). Because a greater portion of the signal received can be attributed to the bottom reflected signal at shallow depths we would expect the impact of bottom reflectance changes on residual errors to be correspondingly greater at these depths.

The one meter calibration data set was used to formulate/derive a two band (TM1, TM2) regression algorithm as shown in Table 7, equation 8. The coefficients are smaller than those derived for the high altitude (10 and 30 m) data sets largely because these latter simulated TM signal values contained a larger sensor gain. The coefficients are, however, nearly proportional to those obtained for the 10 and 30 m two band equations which implies the spectral water depth signatures are not controlled by the spatial sampling frequency. Sun glint portions of each of the seven low altitude transects were truncated for this regression analysis. The correlation coefficient was found to be slightly lower and the standard error slightly larger than in the case of the ten meter data indicating a probable greater influence of bottom reflectance

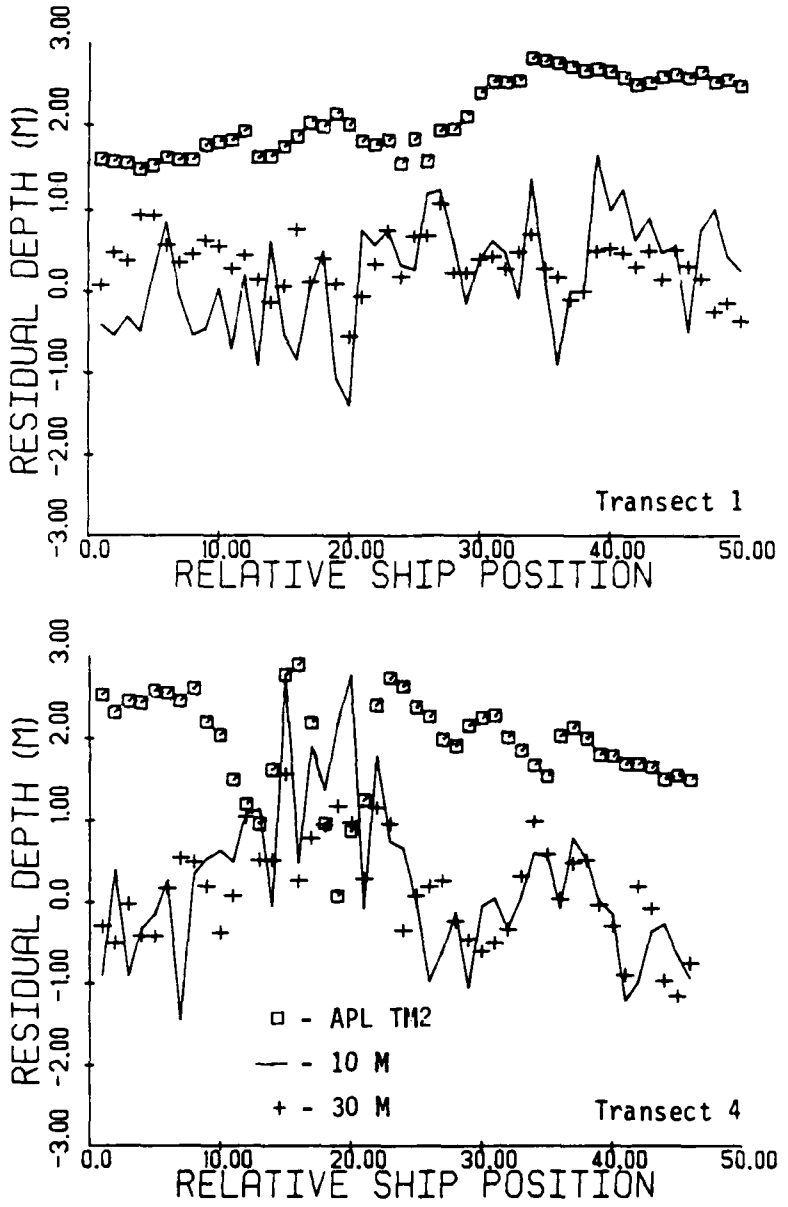

FIGURE 10. TWO BAND REGRESSION RESIDUALS VERSUS TRANSECT POSITION FOR TRANSECTS 1 AND 4

and system noise on the result. The standard error was found to be nearly twice that obtained for the ten meter data when all 131 transect points were used.

4.2 THREE BAND REGRESSION RESULTS

Attempts to define a three band TM algorithm were limited to three band regression using TM1, TM2, and TM3 and the ten and thirty meter calibration data sets. Regression equations and summary statistics are given in Table 9 for mixed and sand bottom types. Regression coefficients for the first two bands are a close approximation to those obtained for the two band case (see Table 7). The coefficients derived for the TM3 band are by comparison to the other bands quite small as were partial correlation coefficients (0.064 - mixed; -0.337 - sand). The third band for this case thus provided no significant contribution to the predicted depth over the range of available calibration water depths. These results suggest that the effective depth range of a three band algorithm is limited to depths less than five meters. A previous study has suggested that TM3 may be less sensitive to bottom reflectance changes for shallow water depths (0-5 m) than TM1 [8]. Furthermore, this study indicated that a TM2, TM3 combination would produce a predicted shallow depth superior to those obtained with any other two or three band combination.

4.3 RATIO ALGORITHM RESULTS

A TM1, TM2 band ratio was used to derive predicted depth equations for mixed and sand bottom types. Ratio equations were derived for both ten and thirty meter resolutions. Results and summary statistics are given in Table 10. It was first attempted to estimate the ratio coefficient from Jerlov reported K values for water type Ia [7] and then estimate the constant term from the calibration data set. Very shallow water TM signals were found to have residual sun glint effects and, therefore, unsuitable for determination of the constant term. In general, it should be possible to calibrate the ratio equation from the TM data independently of the surface truth.

Table 9. Results for Three Band Regression Analysis

Resolution	Bottom Type & Transect Numbers	Regression Equation	Correlation Coefficient	Standard Error (M)
10 meter	Mixed: 1, 6, 7, 9	(1) $\hat{Z} = 6.68X_1 - 11.2X_2 - 0.0136X_3$	0.947	0.917
	Sand: 10, 11, 13	(2) $\hat{Z} = 8.22X_1 - 11.5X_2 - 0.241X_3$	0.956	0.953
30 meter	Mixed: 1, 6, 7, 9	(3) $\hat{Z} = 7.79X_1 - 12.0X_2 - 0.0645X_3$	0.974	0.639
	Sand: 10, 11, 13	(4) $\hat{Z} = 8.65X_1 - 11.1X_2 - 0.341X_3$	0.977	0.661

where $\hat{Z}$ is the predicted water depth

X_i is $\ell n(V_i - V_{si})$ for simulated TM band i

Table 10. Results for Ratio Algorithm

Resolution	Bottom Type Transect Numbers	Band Ratio Equation	Correlation Coefficient	Standard Error (M)
10 meter	Mixed: 1, 6, 7, 9	(1) $\hat{Z} = 9.73\ R_{12} + 5.95$	0.847	1.45
	Sand: 11	(2) $\hat{Z} = 11.6\ R_{12} + 4.66$	0.922	1.25
	Mixed: 1, 6, 7, 9	(3) $\hat{Z} = 11.6\ R_{12} + 4.80$		1.42 (RMS)
30 meter	Mixed: 1, 6, 7, 9	(4) $\hat{Z} = 11.6\ R_{12} + 4.52$		0.94 (RMS)

where $\hat{Z}$ is the predicted water depth (m)

R_{12} is $\ln\left(\frac{V_1 - V_{s1}}{V_2 - V_{s2}}\right)$

Our attempts to calibrate the ratio equation in this manner produced unacceptably large residual depth errors. Two alternative approaches were considered. (1) Use the calibration data directly for a mixed bottom type and linear regression to estimate the coefficients (see Table 10, equation 1). (2) Estimate the coefficient term by regression of the calibration data for a transect with a uniform bottom type (sand).

This latter approach was applied to transect 11 to produce a ratio coefficient value of 11.6 (see Table 10, equation 2). The 11.6 implies a (K1-K2) value of 0.216 which is somewhat larger than the corresponding Jerlov estimate of 0.085. Since TM2 (520-600 nm) lies in a region where the Jerlov K-spectra are changing rapidly it is difficult to estimate a good value of (K1-K2). It is plausible that this large difference could be due to existence of non-Jerlov K spectral shapes or sensitivities of the simulated TM2 band to longer wavelengths. The same ratio coefficient was used to derive a ratio equation for the ten and thirty meter calibration data set (equations 3 and 4, Table 10).

The RMS error of the depth residuals which approximates the standard error of the predicted variable are 50% larger than those obtained with the two and three band regression results, but show the same proportional reduction in standard error from ten to thirty meters resolution.

4.4 ERROR ANALYSIS

Sources of error in the TM depth extraction algorithms include (1) errors in the measured depth, (2) misregistration of the measured and simulated TM data sets, (3) system noise, (4) path radiance changes, (5) sun glint and other surface effects, (6) changes in bottom reflectance, and (7) changes in water clarity type. Errors in the measured depth have been reported by SAI to be less than 0.1 meter. SAI also reported that the positional errors in the sounding data were less than 1.0 meter. The transfer of the ship positions onto the ERIM simulated TM

imagery, although not precisely evaluated, could involve 30 meter errors for the high altitude data set and as much as 50 meters for the low altitude data set (see Table 4). The impact of these latter positional errors could be significant, especially in the shallow waters and where the water depth and bottom cover are changing most rapidly.

Large changes in bottom reflectance as discussed in the previous section can cause predicted depth errors of over one meter. Residual depth error does not appear to be related to depth as indicated by the scatterplot shown in Figure 11. There does appear to be greater dispersion in these residuals at the shallower depths which are related to an increased sensitivity to bottom reflectance changes. If greater depths (>20m) were available for this calibration set we would expect a large dispersion of residual depths, not because of bottom reflectance, but rather due to the increased influence of environmental and system noise.

Errors due to water clarity changes are difficult to define but as discussed in previous work can be expected to be small [8]. Errors due to environmental noise as residual surface effects and path radiance can be lumped together with system noise. A measure of the combined error is the noise in the deep water signal level. The impact of this latter error is evaluated below for the one and ten meter calibration data sets.

An estimate of the depth error resulting from noise in the deep water signal can be obtained by differentiating the water depth regression equation and assuming the noise to be uncorrelated between bands. The total depth error due to deep water signal noise for a single point is given by the following equation.

$$\Delta z = \left[\sum_{i=1}^{N} \left(\frac{b_i \, i \, \sigma 2}{V_i - V_{Si}} \right) \right]^{1/2}$$

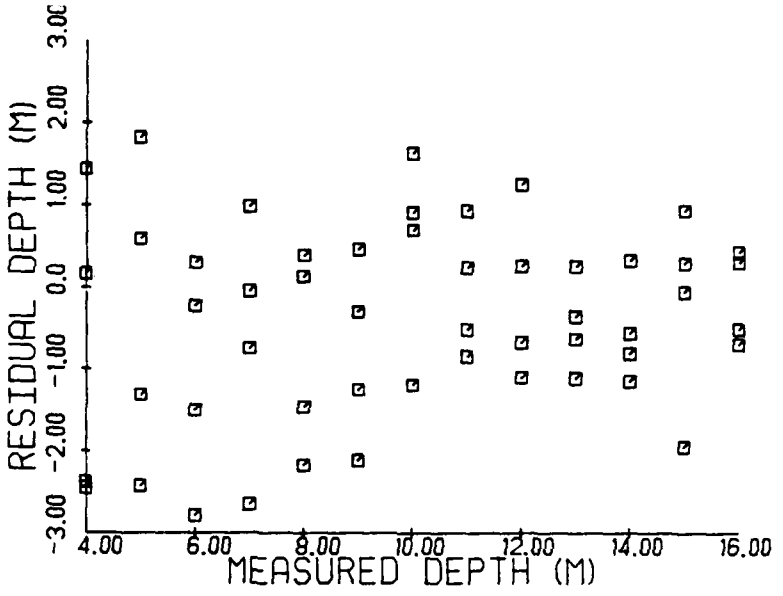

FIGURE 11. RESIDUAL DEPTHS FROM TWO BAND REGRESSION VERSUS MEASURED DEPTHS FOR TRANSECTS 10-13

Here σ_i is the standard deviation of the deep water signal. The RMS error for a given data set can be evaluated by substituting simulated TM signals into the above equation. This analysis was performed for the two band regression algorithms developed from both the high and low altitude Cat Cay data sets. These results can then be compared to the observed depth errors (i.e., residual depths) on a point-by-point basis. Alternatively, one can average such errors over the entire data set and compare the RMS value with the standard error of the predicted depth as obtained from the regression model. Our analysis utilized the standard deviations for the "after sun glint correction" as reported in Table 6. The comparisons shown in Table 11 indicated that much of the observed depth error can be accounted for by the apparent noise in the deep water signal alone. For both the high and low altitude data sets the RMS error implied from the deep water signal noise was based upon the point sets used to derive the regression algorithms.

In the case of the low altitude data set the implied RMS error of 2.02 meters is much larger than the standard error of the prediction at 1.04. In this case, however, the regression algorithm was derived on a subset of points which were located in the glint free area of the image. The RMS residual error of 1.79, as calculated over the entire set of transect points, was found to be more comparable to the implied RMS error due to deep water signal noise. The regression algorithms are applicable over the depth range of the ship transect data and to areas which have been corrected radiometrically for sun glint problems. The RMS errors in the predicted water depth should be on the order of the standard error of the regression estimate. In the case of the high altitude data, the RMS residual depth error was calculated to be 0.883 meters which is comparable to the standard error of 0.868 meters.

For the low altitude data set it appears that the deep water signals used to estimate the noise term may have been influenced by some residual sun glint problems. In any case, sun glint is a more severe

TABLE 11

COMPARISON OF CALCULATED AND
OBSERVED DEPTH ERRORS

High Altitude, 10 meter resolution

b_i = 6.64, -11.3

σ_i = 3.92, 1.46

standard error = 0.868 meters

observed RMS = 0.883

Low Altitude, 1 meter resolution

b_i = 1.75, -3.81

σ_i = 10.21, 3.13

standard error = 1.04 meters

observed RMS = 2.02

problem with the low altitude data set. Furthermore, the residual effects limit the applicability of the water depth algorithm to portions of the image which are both in the depth range of the transects and glint free.

The APL photometer data were used to normalize the simulated TM signals so as to attempt to minimize the influence of bottom reflectance changes on the predicted depth result. The normalization factors were estimated for TM1 and TM2 by first converting the APL reading to a quantity which was considered to be proportional to bottom reflectance. These values were then expressed as a ratio with their mean value as described by the following equations.

$$N(\lambda) = L_u(\lambda) + (R_B(\lambda)/\pi - L_u(\lambda))\, e^{-2k(\lambda)z} \qquad \text{[ref. 9]}$$

$$R_B(\lambda) = \pi((N(\lambda) - L_u(\lambda))/e^{-2k(\lambda)z} + L_u(\lambda))$$

$$R^*(\lambda) = \frac{\text{MEAN}\,(R_B(\lambda))}{R_B(\lambda)}$$

where L_u is the APL radiometer upwelling signal received over deep water or a bottom type with very low reflectance, N is the reported calibrated radiometer value, R_B is a quantity proportional to actual bottom reflectance, and R* is the bottom normalization factor (relative change in bottom reflectance). These latter normalization factors were evaluated for each point on the ship transect and multiplied by the corresponding value of $V_i - V_{si}$. A new value of X_i was computed for each point of the calibration set and subsequently, used to derive a new two band regression depth equation (equation 5, Table 7).

Application of this two band depth equation to transects 1 and 4 produced residual depth errors which are plotted in Figure 12. Also plotted are values of R_B. Comparison of these residuals with those shown previously in Figure 10 show that this normalization process

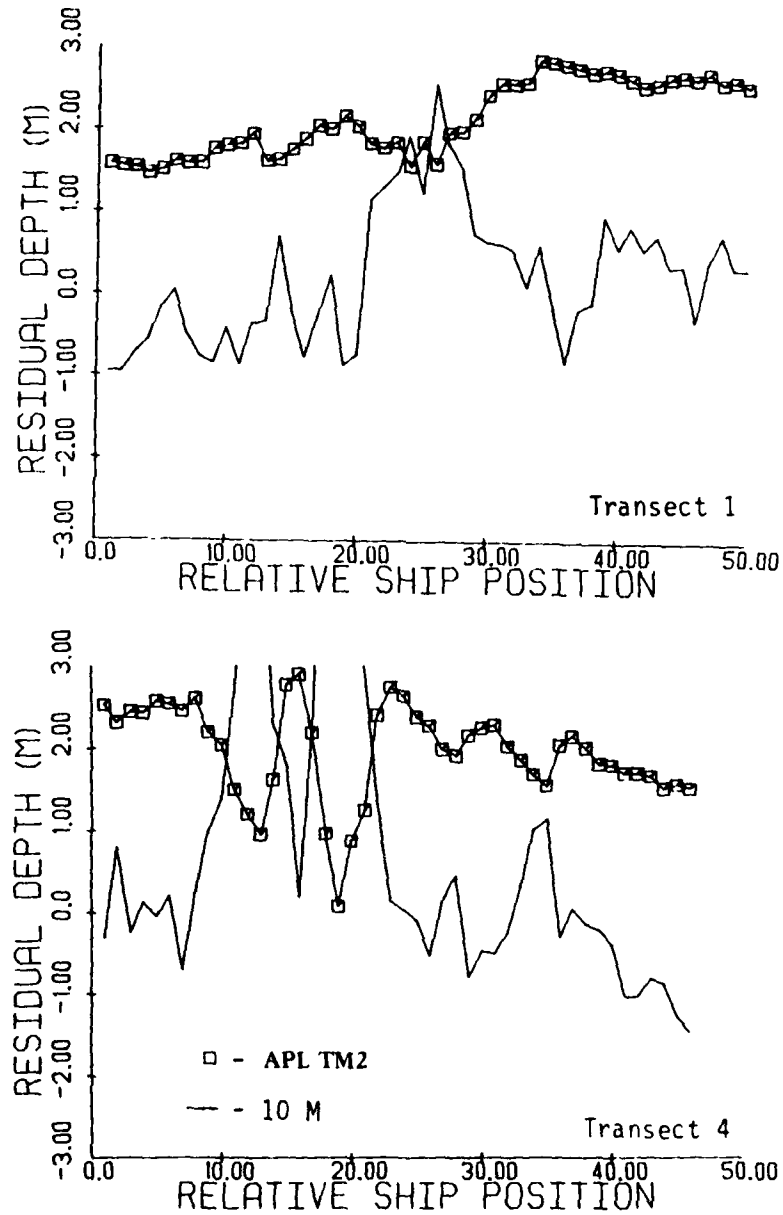

FIGURE 12. TWO BAND REGRESSION RESIDUAL DEPTHS AFTER ADJUSTMENT FOR BOTTOM REFLECTANCE CHANGES

increased the residual errors rather than reduced them. It appears that the APL photometer readings are far more sensitive to changes in bottom reflectance than those obtained from the aircraft multispectral data. Precise alignment of simulated TM data with the APL photometer measurements is also critical to obtaining good results with this normalization approach and, therefore, misalignment may account for some of the discrepancy.

4.5 DEPTH PROCESSING PROCEDURES

The overall data processing and analysis procedures are outlined with the flow diagram shown in Figure 13. The details of most of these steps have been discussed previously in section 3.0. The actual depth processing was carried out using ERIM's QLINE image processing program. A depth calculation program was constructed for this system which can be used to calucate a water depth for each pixel based on selected two band, three band, and ratio algorithms. Processing for the ten meter resolution was conducted using this program and the two band, three band, and ratio depth equations (respectively, equation 1 of Table 7; equation 1 of Table 9; and equation 3 of Table 10). Processing was also conducted for the thirty meter resolution using a complementary set of three equations (equation 4 of Table 7, equation 5 of Table 9, and equation 4 of Table 10). No pixel-by-pixel processing of the low altitude one meter data was made since there was insufficient time to construct the production numerical overlays.

Water depths were calculated for each algorithm where each of the required bands had a signal level at least one count greater than the deep water threshold (Table 6). Predicted depths for each algorithm affected by a signal level falling below this threshold were set to a zero value. If TM4 was found to be greater or equal to the land and higher sun glint threshold (i.e., TM4 = 254) then the predicted depth for each algorithm was set to zero. The output water depths were scaled to integer values ranging from 0 to 255 representing depth in tenths of

FIGURE 13. SIMULATION OF TM DATA AND DEPTH PROCESSING

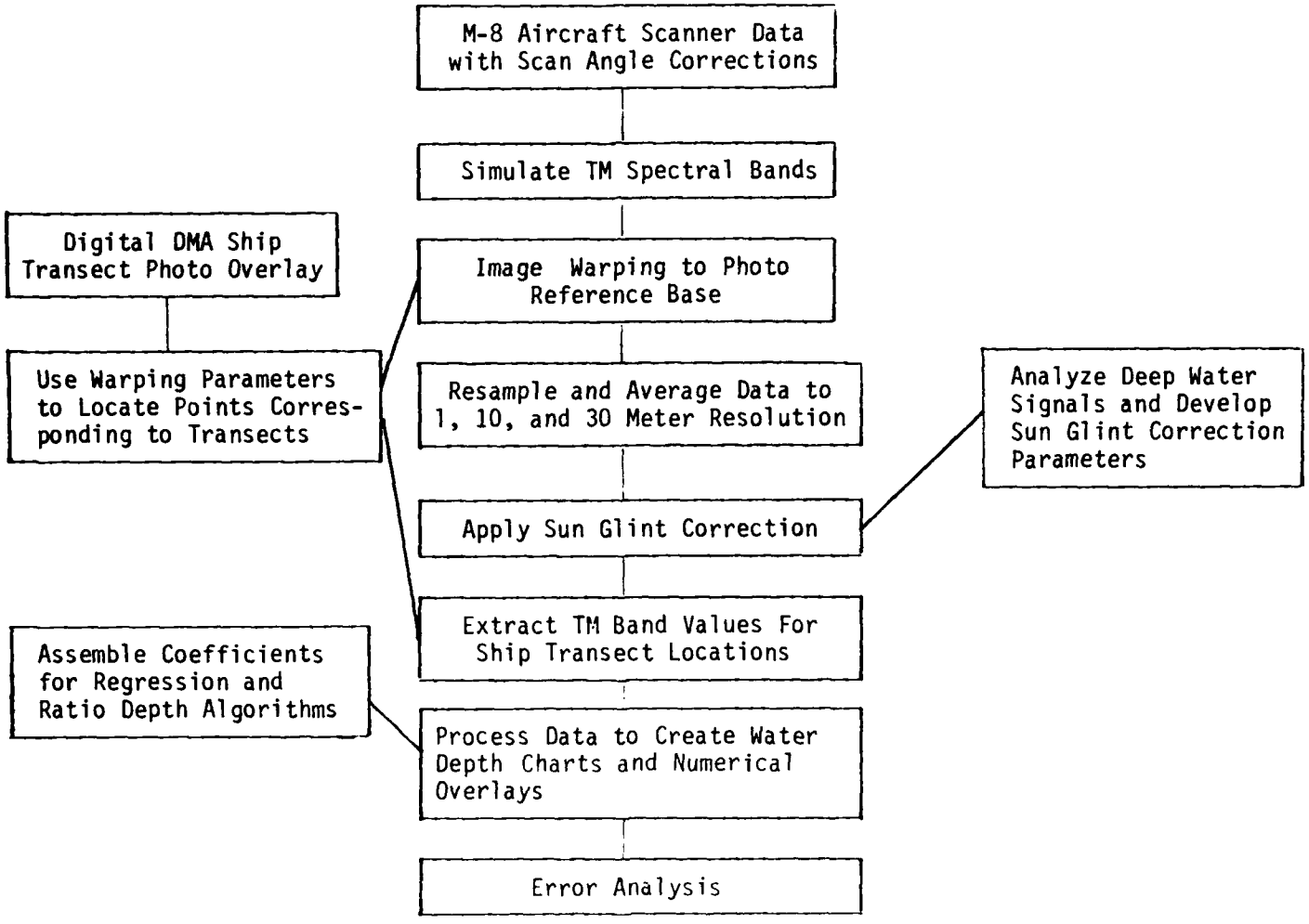

a meter. In order to display a chart of these depths they were categorized into one and two meter intervals as described in the next section.

4.6 GENERATION AND INTERPRETATION OF OVERLAY PRODUCTS

Under this program a series of transparent depth maps and overlays have been produced to allow image interpretation of spatial patterns in bottom type vegetation and its influence on calculated water depth. All of the products have been generated for the Cat Cay study area and all have been produced to a common scale (approximately 1:8,000). Depth maps and overlays were constructed only for the high altitude data set. The transparent depth maps were made for subareas 1 and 2 which essentially constitute the upper and lower portions of the 1980 Photobathymetric Calibration Survey Area (see Figure 14). The black and white depth maps were made with 13 distinct grey tones which correspond to the water depth ranges shown in Table 12.

TABLE 12

CATEGORIZED WATER DEPTHS FOR DEPTH MAPS

GREY LEVEL	WATER DEPTH RANGE (M)
0 (Black)	Land
1	25
2	20.0 - 24.9
3	17.0 - 19.9
4	15.0 - 16.9
5	13.0 - 14.9
6	11.0 - 12.9
7	9.0 - 10.9
8	7.0 - 8.9
9	6.0 - 6.9
10	5.0 - 5.9
11	3.0 - 4.9
12 (White)	0.0 - 2.9

Separate depth charts were generated for the three band regression algorithm, the two band algorithm, and the ratio algorithm for both ten and thirty meter resolution (see Figures 15 through 17). In addition to

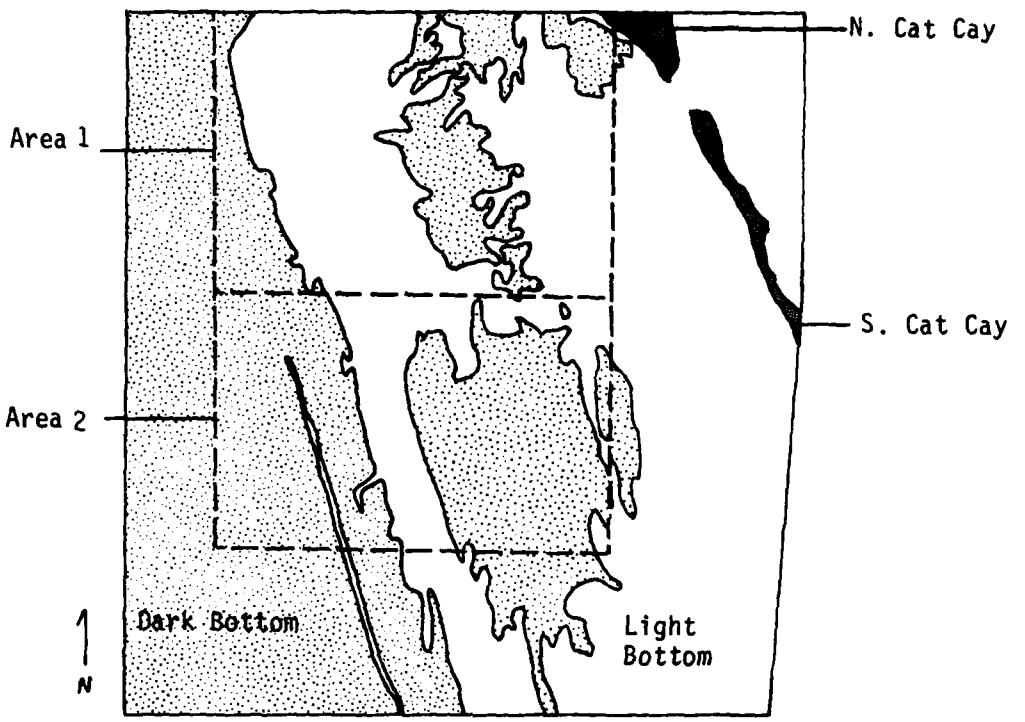

FIGURE 14. DEPTH PROCESSING AREAS FOR CAT CAY HIGH ALTITUDE DATA SET (PHOTO #0065)

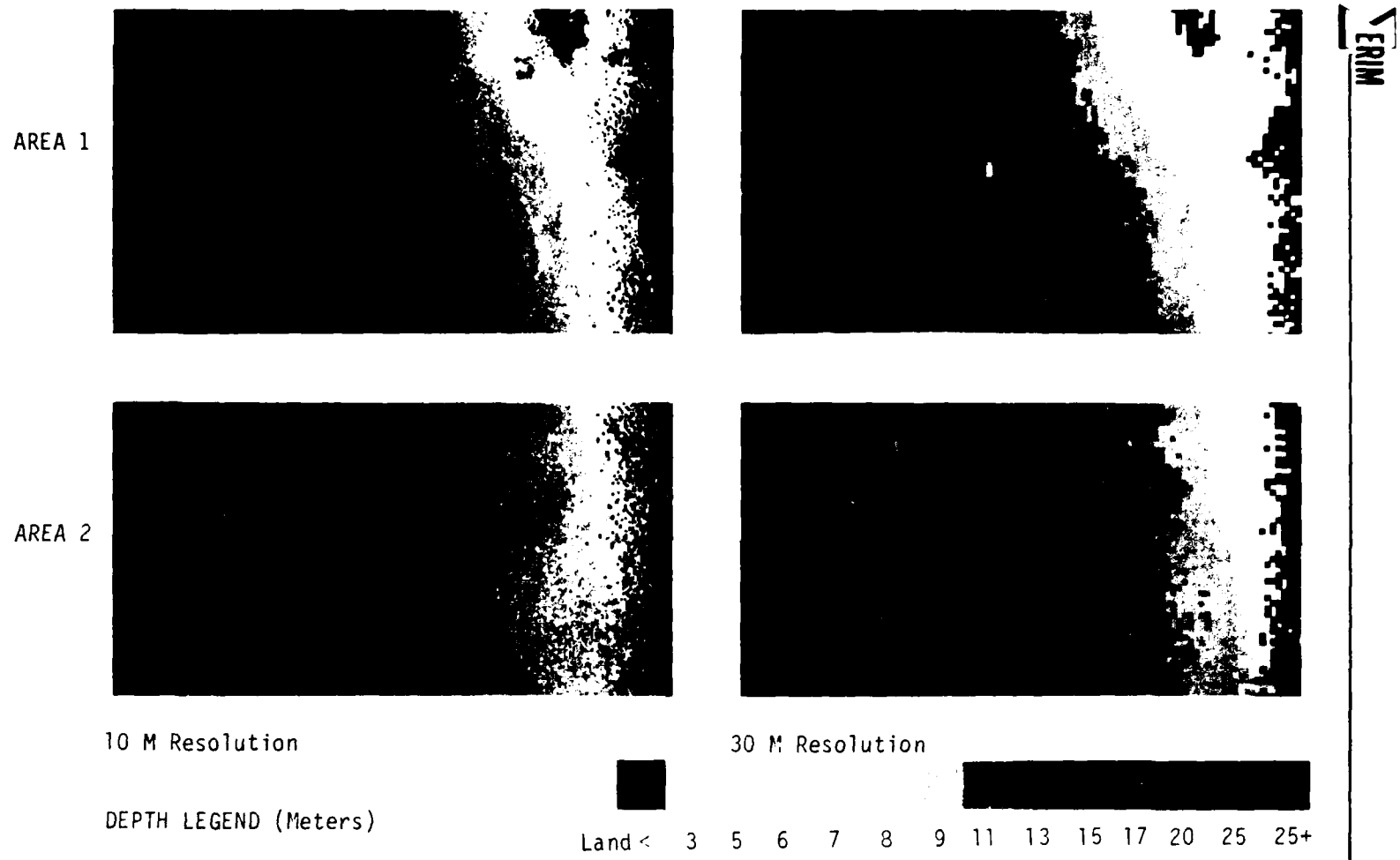

FIGURE15.DEPTH CHARTS FOR CAT CAY SUBAREAS USING TWO BAND REGRESSION ALGORITHM AND SIMULATED TM DATA

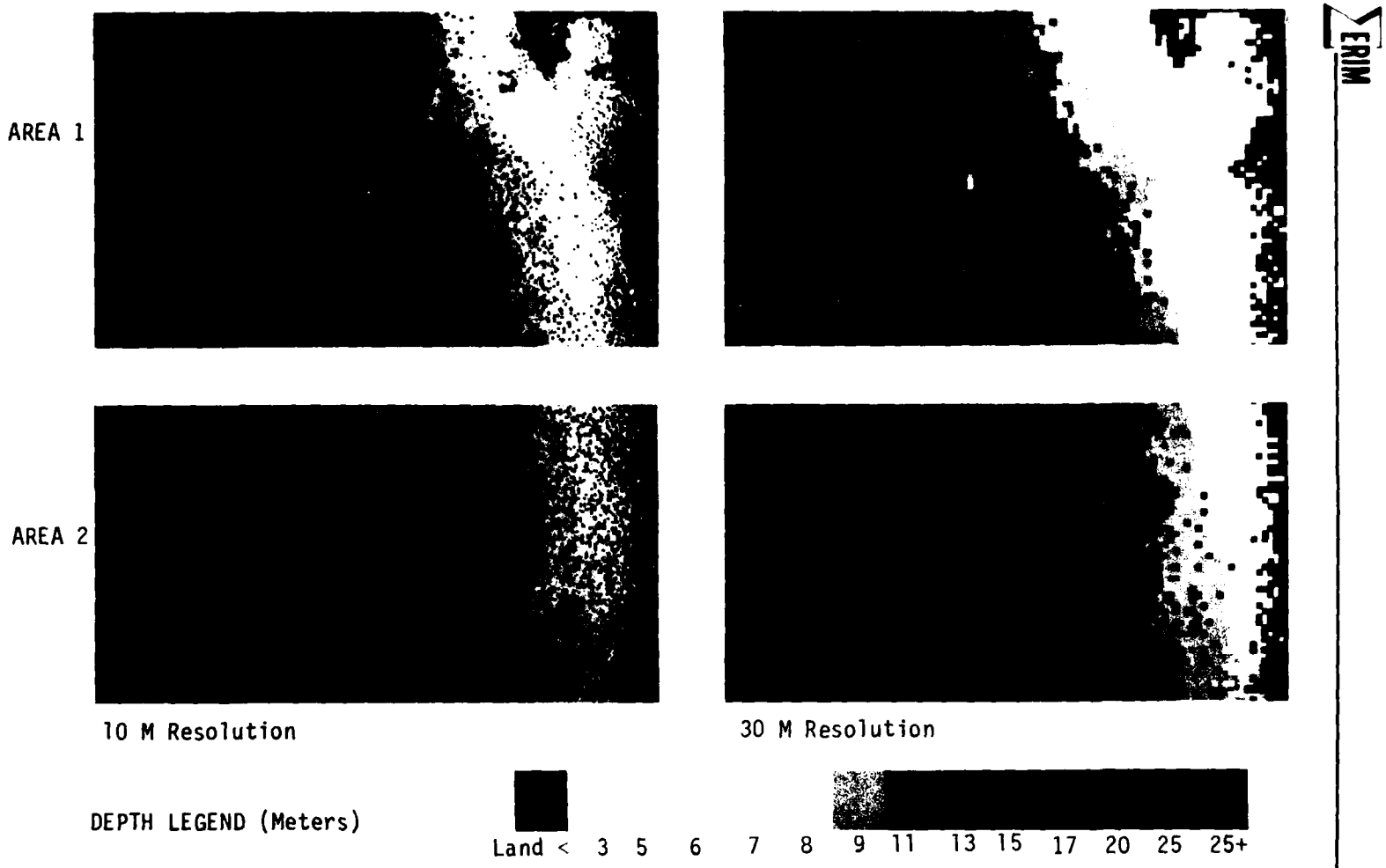

FIGURE 16. DEPTH CHARTS FOR CAT CAY SUBAREAS USING THREE BAND REGRESSION ALGORITHM AND SIMULATED TM DATA

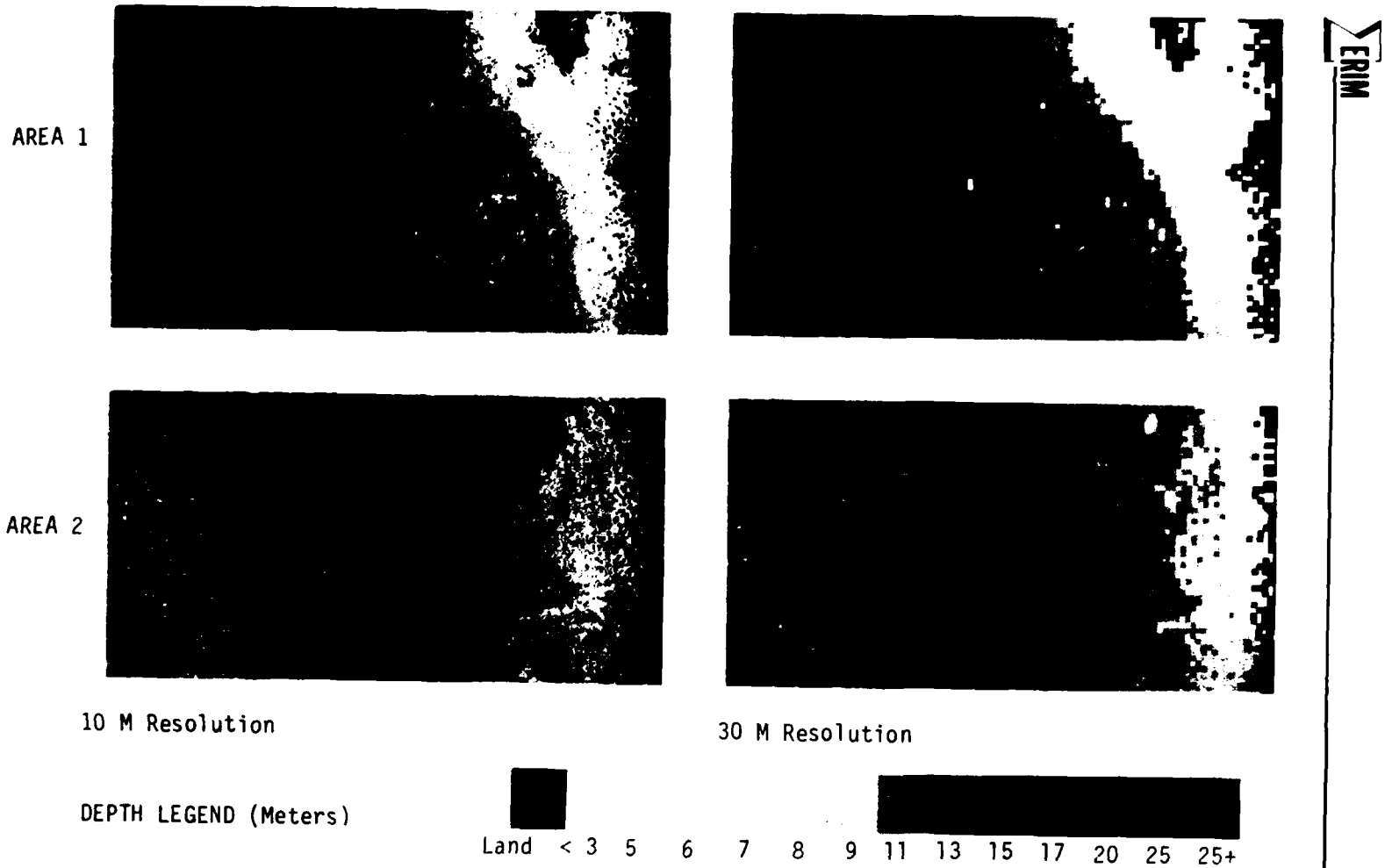

FIGURE 17. DEPTH CHARTS FOR CAT CAY SUBAREAS USING RATIO ALGORITHM AND SIMULATED TM DATA

the transparencies, a series of ten overlay maps were generated for the Cat Cay area. These overlays were designed to show predicted water depths on a regular grid or residual depths (measured minus predicted) along the calibration transects.

A computer plotting program was developed to generate the overlays which were calibrated to produce maps at the precise scale of the photo product to be used as the base map (approximately 1:8,000). The precise location of the depth value is indicated, by convention, according to the decimal point. Overlays were produced showing predicted depths from the two band algorithm on a regular five or fifteen pixel (50 or 150 meter spacing) grid. In addition, in order to indicate performance of the algorithm along the transect, a series of overlays were made showing the residual depths. Overprinting of the plotted values on the individual transects (which would render the depth values unreadable), was avoided by constructing separate overlays for alternating values. The plotted maps were converted from paper plots to transparent overlays using standard photographic techniques. The precision in constructing these overlays was estimated to be two millimeters in the final product. Comparison of the locations of residual points on the ship transects to those plotted (by hand) in constructing the original DMA overlay shows good agreement. Where small discrepancies in sounding location between the two overlays exist, they are due primarily to errors in the pixel extraction procedure which has been previously stated to be accurate to within approximately two pixels. Orientation of the transparent overlay on the base map is as follows. The origin of the overlay corresponds to the upper right hand corner (NE) of the base map with points increasing to the left and lines increasing downward. It should be noted that the point axis has been reversed from its normal orientation (i.e., points increasing to the right). A list of overlays and water depth maps produced is shown in Table 13.

TABLE 13

PRODUCT DEPTH MAPS AND TRANSPARENT OVERLAYS FOR
THE CAT CAY CALIBRATION AREA

GREY TONE DEPTH MAPS (1:8,000)

1. Two Band Regression, 10 M, Area 1
2. Two Band Regression, 10 M, Area 2
3. Two Band Regression, 30 M, Area 1
4. Two Band Regression, 30 M, Area 2
5. Three Band Regression, 10 M, Area 1
6. Three Band Regression, 10 M, Area 2
7. Three Band Regression, 30 M, Area 1
8. Three Band Regression, 30 M, Area 2
9. Ratio Algorithm, 10 M, Area 1
10. Ratio Algorithm, 10 M, Area 2
11. Ratio Algorithm, 30 M, Area 1
12. Ratio Algorithm, 30 M, Area 2

TRANSPARENT OVERLAYS (1:8,000) WITH NUMERICAL VALUES AS PREDICTED WITH THE TWO BAND REGRESSION ALGORITHM.

1. Regular 15 Pixel Grid, 10 M, Area 1
2. Regular 15 Pixel Grid, 10 M, Area 2
3. Regular 15 Pixel Grid, 30 M, Area 1
4. Regular 15 Pixel Grid, 30 M, Area 2
5. Regular 5 Pixel Grid, 10M, Area 1
6. Regular 5 Pixel Grid, 10M, Area 2
7. Residual Depths for Ship Transects, 10 M, Part A
8. Residual Depths for Ship Transects, 10 M, Part B
9. Residual Depths for Ship Transects, 30 M, Part A
10. Residual Depths for Ship Transects, 30 M, Part B

The grey tone depth charts shown in Figures 15, 16, and 17 for the two band, three band, and ratio algorithms provide a means to examine the spatial effects of resolution and algorithm sensitivity to bottom features and environmental noise. The photo maps for the three band algorithm clearly shows the depth limits for application. Detail in the very shallow depths is limited by land mass or band saturation. For this three band algorithm reliable depths could be calculated to a depth of eight to ten meters where band 3 becomes severely impaired with environmental noise as indicated by the high density of black pixels. Notice that for the thirty meter resolution case the averaging process has reduced the environmental noise significantly allowing greater depths to be defined. For reasons previously stated the two band results are essentially the same as those obtained for the three band algorithm except for the impact of environmental and system noise. Patterns of dense bottom vegetation which are apparent in the simulated data sets (Figures 4 through 6) also appear to some extent in the ten meter depth map for subarea 1 (Figures 15 through 17). The lower bottom reflectance in these areas produced lower signal levels for both bands one and two resulting in a greater predicted water depth. These same features are essentially eliminated in the thirty meter TM depth charts. Also note the anomalous feature in the central portion of subarea 1 data set which was sufficiently bright to be classified as land (black) in the ten meter case. There is a similar feature present in subarea 2 map near the bank margin consisting of only a single ten meter pixel. These same bright pixels were averaged with adjacent pixels having much lower signal levels to reduce the brightness of this feature sufficiently so that it was interpreted as shallow water (white) in the thirty meter depth charts. This latter comparison suggests that the Thematic Mapper will be capable of detecting temporal hazards which have high reflective properties or high depth contrast and also possess physical dimensions which could be smaller than a single TM pixel.

The water depth charts produced from the ratio algorithm appear to be substantially more noisy than those produced with the two band regression technique. This increase in noise is especially visible in the deep water areas. The bottom features and anomalies discussed above are also visible in the ratio processed charts. The predicted depths over the dark bottom features in subarea 2 are shown to be shallow water (light grey tone) which is just the opposite result from that obtained with the regression algorithm. Apparently the bottom reflectances are not proportional for these bottom types as assumed for independence in the ratio algorithm. Furthermore, these results suggest that the bottom reflectance in the blue-green (TM1) band decreased more than the green (TM2) band over these vegetated areas resulting in the prediction of relatively shallow water depths. This suggested relative change in reflectance is consistent with reported shapes of bottom spectra for Turtle grass, Manatee grass and other "green" bottom types as compared to that of a sand bottom [8]. Most of the depth anomalies due to bottom cover type are removed in the thirty meter depth chart. More are visible, however, than was the case for the two band regression charts.

The transparent overlays with grids of numerical predicted depth values show the same sensitivities of the two band regression algorithm to bottom type as with the depth charts. These numerical overlays can be used to quantify the impact of predicted depth anomalies due to bottom cover, in some cases, by comparing the ten and thirty meter results.

In summary, it appears from these data that small changes in bottom reflectance and small areas of anomalous bottom type will have minimum impact on the predicted depth as obtained from TM data.

5.0

CONCLUSIONS AND RECOMMENDATIONS

This study simulated the TM spectral and spatial resolutions using aircraft M-8 scanner data for the primary purposes of developing or revising existing depth extraction algorithms to accept and utilize TM data. Conclusions and recommendations follow.

5.1 GENERAL CONCLUSIONS

Both the spatial and spectral resolutions of the Thematic Mapper appear to be appropriate for remote bathymetry. The bottom cover type was found to influence the predicted depths, especially with the one and ten meter resolution aircraft data. Many of these same unwanted bottom effects were essentially eliminated in the thirty meter pixel depth chart. For the Cat Cay calibration area it appears that the TM spatial resolution of 30 meters would produce water depth charts which are less influenced by bottom reflectance changes and therefore more accurate than those charts which would be obtained using a higher spatial resolution. Results from this study suggest that, outside of the problem of spatial variability of haze (aerosols), environmental noise is greater for higher spatial resolutions due principally to surface effects. Thus, the use of higher resolutions may be only warranted in cases where it is necessary to detect and chart a rapidly changing water depth (point hazard).

5.2 SPECIFIC CONCLUSIONS

A two band regression algorithm using TM bands one and two was found to be the best algorithm (correlation coefficient = 0.948, standard error = 0.868 m for a depth range of 4-15 m) for the simulated data sets and available surface truth. A three band regression algorithm (see Equation 1, Table 9) was developed (correlation coefficient = 0.947, standard error = 0.917 m) but could not be effectively tested since the ship soundings did not extend to sufficiently shallow depths.

Because of the limits of light penetration, it is not likely that a three band algorithm would be superior to a two band algorithm beyond four or five meters depth for this water. The spectral resolution of TM will allow a two band algorithm to operate to depths in excess of twenty meters and a three band algorithm to a maximum depth of ten meters.

The ratio algorithm (TM1/TM2) produced the largest errors (correlation coefficient = 0.847, standard error = 1.45 m) in predicted depth and was found to be sensitive to changes in bottom reflectance. These errors resulting from bottom reflectance indicate that ratios of reflectances in these two TM bands are not equal for this set of bottom types.

The image warping techniques utilized under this program were found to be a viable approach to merging the ship soundings with the simulated TM data. These techniques are especially useful where there is insufficient or unreliable information needed to place both data sets in a common geographical reference system. However, the spatial errors associated with this merging process could not be easily traced since both analog and digital processes were involved.

The two band regression algorithm had smaller residual errors for the simulated thirty meter resolution (standard error = 0.612 m) than for the nominal ten meter resolution (standard error = 0.868m). This was due principally to the system and environmental noise reductions obtained with the averaging process used to generate the thirty meter resolution from the ten meter data. These noise levels for the simulated data are not necessarily representative of those which are characteristic of actual TM data. Furthermore, it is not known as to what portion of these noise components are due to atmospheric variations. Thus, the relative performance of these algorithms with actual TM data will depend highly on the relative size of the system and environmental noise components.

The one meter low altitude data were found to have the largest relative noise components and produced predicted depths with the largest

residual errors (standard error = 1.04 m) relative to the ten and thirty meter resolutions. Using all of the transects depths, environmental and system noise components for the one meter data set were found to be nearly twice that of the ten meter data set. Because of the large noise component which remained after the sun glint correction was applied, attempts to reduce the resolution of the low altitude data from one to thirty meters did not produce meaningful results.

5.3 RECOMMENDATIONS

Research should be initiated to model the coefficients and constant term of the chosen/recommended regression depth algorithm in terms of local atmospheric and surface conditions. Ideally these conditions should be normalized radiometrically on a pixel by pixel basis. In addition, the influence of bottom type and water clarity should be considered. Once we can model the coefficients in the algorithm, or at least learn how the coefficients change with environmental conditions, then a TM depth extraction algorithm can be proposed which can operate independently of a large ship or aircraft data base.

A two band algorithm using TM1 and TM2 (Table 7, Equation 1) is the recommended algorithm for water depth extraction using Thematic Mapper data as input. A three band algorithm could offer a more precise water depth prediction for shallow waters of less than five meter depths. If an improved prediction capability is desired for these depths, then a supplemental set of water soundings should be collected in shallow water for purposes of calibration.

The two band regression algorithm developed in this study can be used with actual TM data only after it has been calibrated to surface truth. For the Cat Cay area the radiometric differences between the simulated data set and actual TM data are anticipated to be large enough to warrant recalibration to the ship sounding data base.

REFERENCES

1. E. Doak, J. Livisay, D. Lyzenga, J. Ott, and F. Polcyn, Evaluation of water depth extraction techniques using Landsat and aircraft data, ERIM Report No. 135900-2-F, January 1980.

2. D.R. Lyzenga, Coastal remote sensing investigations, Volume 1: multispectral bathymetry analysis, ERIM Report No. 134400-11-F, April 1980.

3. D.R. Lyzenga, J.S. Ott, J.P. Livisay, and F.C. Polcyn, Remote bathymetry with a multispectral active/passive airborne system, ERIM Report No. 149600-1-F, February 1982.

4. Cook, G.S., et al., "Cruise Report 1980 DMA Bahamas Photobathymetric Calibration Survey," Volume I, Technical Summary of SAI Program, October 15, 1980.

5. Stewart, L.L. Preliminary Report on the Photobathymetric Calibration Project Great Bahama Bank, 7 July-2 August 1980, University of Connecticut, Marine Sciences Institute, September 1980.

6. F.C. Polcyn, F.J. Tanis, and J.P. Livisay, Photobathymetric calibration project Great Bahama Bank, July-2 August 1980, ERIM Report 154100-9-F, May 1982.

7. N.G. Jerlov, Optical Oceanography, Elsevier Pub. Co., Amsterdam, 1968.

8. F.J. Tanis. Radiance calculations for optimization of sensors designed for remote bathymetry, Volume 1, ERIM Report No. 155800-1-F, July 1982.

9. Walker, R.E. and B.F. Hochheimer. Operation and calibration of the APL/JHU photometer for DMA multispectral bathymetry project. John Hopkins University, Applied Physics Laboratory, June 1979.

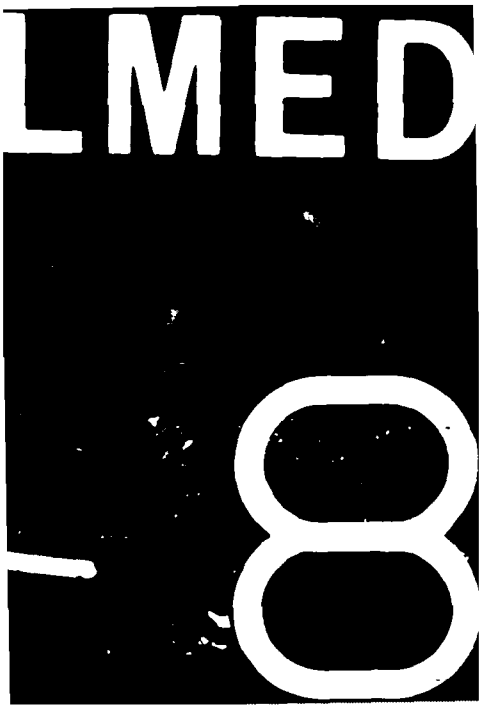
LMED
8